The Dissertation Committee for Wei-Shun Chang Certifies that this is the approved version of the following dissertation :

Single Molecule Study on the Conformation, Orientation and Diffusion Anisotropy of Conjugated Polymer Chains in a Liquid Crystal Matrix

Committee:

Paul F. Barbara, Supervisor

Peter J Rossky

David A. Vanden Bout

Keith J. Stevenson

Zhen Yao

Single Molecule Study on the Conformation, Orientation and Diffusion Anisotropy of Conjugated Polymer Chains in a Liquid Crystal Matrix

by

Wei-Shun Chang, B.S.; M.S.

Dissertation

Presented to the Faculty of the Graduate School of
The University of Texas at Austin
in Partial Fulfillment
of the Requirements
for the Degree of

Doctor of Philosophy

The University of Texas at Austin
December, 2007

Dedication

To my family

Acknowledgements

I would like to thank my supervisor Professor Paul Barbara, who is enthusiastic in scientific research and always inspires students and postdoctoral researchers working with him. The knowledge and working attitude I learned from him help me tremendously to build up the foundation on my research career. I am also very lucky to work with some talented colleagues in Paul's group, especially with Dr. Stephan Link. Stephan helps me on developing the research project in this dissertation. I like to thank Dr. John Grey and Dr. Rodrigo Palacios for the cooperation on the SMS-EC projects. I also like to thank all members in Paul's group for sharing the knowledge and experience on the research and life. Finally, I want to thank my wife Susanna and my son Minhong for their support on my life to finish my degree.

Single molecule study on the conformation, orientation and diffusion anisotropy of conjugated polymer chains in a Liquid Crystal Matrix

Publication No._____________

Wei-Shun Chang, Ph.D.
The University of Texas at Austin, 2007

Supervisor: Paul F. Barbara

The nature of the solvent plays an important role in the conformation and orientation of polymers in solution. A particularly interesting case is when the solvent itself possesses order, such as when dissolving the polymer in a LC. In this dissertation, the morphology and diffusion behavior of the conjugated, stiff polymer MEH-PPV, (poly[2-methoxy-5((2-ethylhexyl)oxy)-1,4-phenylenevinylene]), in liquid crystal (LC) solvents have been investigated. Using polarization sensitive fluorescence correlation spectroscopy, it was found that in a nematic LC the polymer molecules are extended and highly aligned parallel with the nematic director. The conformation and orientational order of MEH-PPV increase with chain stiffness as a result of an interplay among the conformational entropy, solvation anisotropy, and bending energy of the polymer chains. In the smectic phase, about 10% of the MEH-PPV molecules are aligned perpendicular to the director in between the smectice layers, an effect not previously observed for a polymer solute. When applying an external electric field across the LC cell, the LC director changes orientation from a planar to a homeotropic alignment. The MEH-PPV chains remain aligned parallel with the LC director with applied field in the bulk of the LC device. However, the local structure near the LC-substrate interface is more complex. Single molecule polarization distributions measured as a function of distance from the LC device interface allow us to use MEH-PPV as sensitive local probe to explore complex structures in anisotropic media. Furthermore, diffusion anisotropy of the polymer solute in a LC solvent was studied by a novel two-beam cross-correlation technique. The diffusion anisotropy was observed to be about 2. This value is comparable to the diffusion anisotropy of the solvent and suggests that, despite the high degree of alignment, the solute diffusion is governed by the solvent and not the solute.

Table of Contents

List of Tables

List of Figures

Chapter 1: Introduction

1.1 CONJUGATED POLYMERS

Conjugated polymers represent a novel class of nano-electronic materials, with potential applications as organic light emitting diodes, photovoltaics, or chemical sensors.[1-3] The continued interest in developing devices composed of conjugated polymers arises from their ease of processing and low cost. One important class of the conjugated polymer is Poly(phenylene-vinylene) (PPV) whose structure is shown in Figure 1.1. The overlap of the π orbitals along the carbon backbone causes the delocalization of electrons, which results in the unique electrical and optical properties of the conjugated polymer. Spectroscopically, one can define a chromophore which is a segment of the conjugated polymer that can absorb and emit light, i.e. the length of electronic delocalization. The length of an individual chromophore in PPV is 10~15 repeat units. A single polymer, poly[2-methoxy-5-(2'-ethyl-hexyloxy)-1,4-phenylene vinylene] (MEH-PPV), with molecular weight of 100,000 is comprised of ~400 repeat units and therefore ~ 40 chromophores. Photo excitation of a conjugated polymer generates excited species (or excitons) on individual chromophores. The interactions

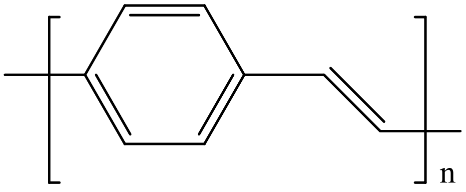

Figure 1.1 Molecular structure of PPV

between multiple excitons on a single chain are very complicated in comparison to molecular chromophores or inorganic nanostructures such as quantum dots, and this complication influences the electronic properties of the polymer, such as band structure, emitting states, and quantum efficiency. The complexity is attributed to fluorescence from both intra- and inter-chain contacts. Polymer conformation and orientation plays an essential role in the observed photophysical properties of conjugated polymers,[4-10] thereby suggesting interesting strategies for optimizing their electronic properties.

Some efforts have been made to enhance the conformation and orientation order[5,11-15] of polymers. For MEH-PPV, it has been reported that it can be assembled uniformly with the long axis oriented perpendicular to the substrate by an ink-jet printing technique[5,15]. The well-defined spacing and orientation of individual polymer molecules achieved by this printing technique is important for easy processing of nanostructured materials without the need for a template [5,15]. The conformation of MEH-PPV can also be varied by introducing tetrahedral defects along the polymer backbone[7,10,16] and through the polarity of the solvent[17,18]. Using single molecule excitation polarization spectroscopy together with Monte Carlo (MC) simulations, the conformations of MEH-PPV in a supporting polymer matrix was shown to be those of a defect coil and a defect cylinder when considering the presence of a small number of tetrahedral defects[7,10,16]. These simulated conformations are highly ordered structures giving rise to large optical anisotropies in agreement with the experimental results. With increasing concentration of tetrahedral defects, MEH-PPV loses its conformational order and assumes a molten globule or random coil conformation[16]. It was further observed that MEH-PPV retains its solution phase conformation after spin-casting a dilute solution onto a glass substrate[17,18]. Polymers initially dissolved in a polar vs. a nonpolar solvent were found to be predominantly in an extended and collapsed conformation after solvent evaporation, respectively. These investigations suggest that the conformation of MEH-PPV can be controlled by the number of defects and the nature of the solute-solvent interaction. A particularly interesting case is when the solvent itself possesses order, as is in the case of a liquid crystal (LC). This dissertation focuses on the conformation, orientation and diffusion anisotropy of conjugated polymers in the LC matrix. In the next section, the basic physical properties of LCs will be discussed.

1.2 LIQUID CRYSTAL

1.2.1 PHYSICAL PROPERTIES OF LIQUID CRYSTAL

Liquid crystal (LC) is a state of matter intermediated between the isotropic liquid and crystalline solid. With this intermediate property, the LC molecules lack a short distance translational order like a crystalline solid does, but have a long distance orientational order. The long distance orientation order defines anisotropic properties such of optical, electric and magnetic properties of the liquid crystal which have attracted a great interest not only in the fundamental sciences but in technological applications.

LCs are divided into two categories, lyotropic LCs and thermotropic LCs, depending on the mechanism of the phase transition from the isotropic phase to the LC phase. The phase transition for the lyotropic LC is due to the change in the concentration of the LC molecules while that for the thermotropic LC is due to the change of the temperature. In this dissertation, a thermotropic LC was used as a solvent. Most known thermotropic LC are formed by organic compounds with an elongated shape such as rod-like or disk-like molecules. Many of them are aromatic composed of two or more benzene rings as a core and an alkyl group as a tail.

The main subdivisions for the thermotropic LC for the elongated molecules at room temperature are the nematic and smectic LC as shown in Fig 1.2 and 1.3. In the nematic phase, the centers of the mass of molecules have three dimensional translational degrees of freedom and are randomly distributed. Therefore they lack translational order, but the molecules are aligned with a reference axis within a domain. In this sense the nematic phase can be referred to as an anisotropic fluid. Most nematic LCs are uniaxial, i.e. one of the axes is longer and preferred and the other two axes are equivalent. Some nematic phases are biaxial meaning that the two short axes are not equivalent.[19] The uniaxial property in refractive index and the dielectric constant of the nematic phase are important for the electro-optic applications. The refractive index difference between the long axis (extraordinary axis) and short axis (ordinary axis) is called birefringence which cause a polarization alteration when light pass through the nematic LC[20]. The dielectric (magnetic) anisotropy is the dielectric constant (magnetic susceptibility) difference between the long and short axes of the molecules which results in a torque force to realign the LC molecules when applying an external electric or magnetic field.[20-22] These physical properties are the foundation of the LC display applications.

The smectice phases, unlike the anisotropic fluid, are characterized by an additional translational order for at least one dimension. The centers of the molecules are, on average, arranged in equidistant planes and are often considered

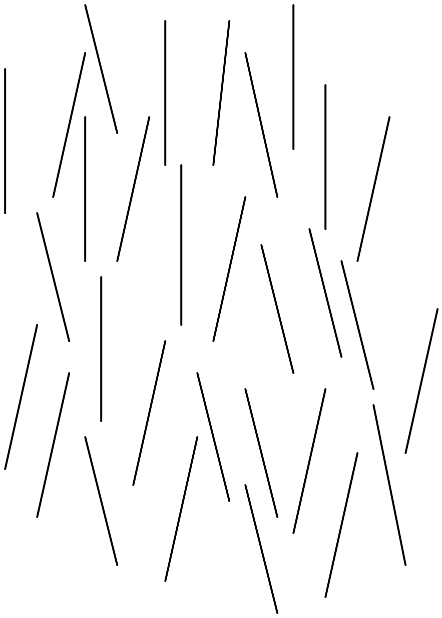

Figure 1.2 Schematic picture of a nematic LC phase.

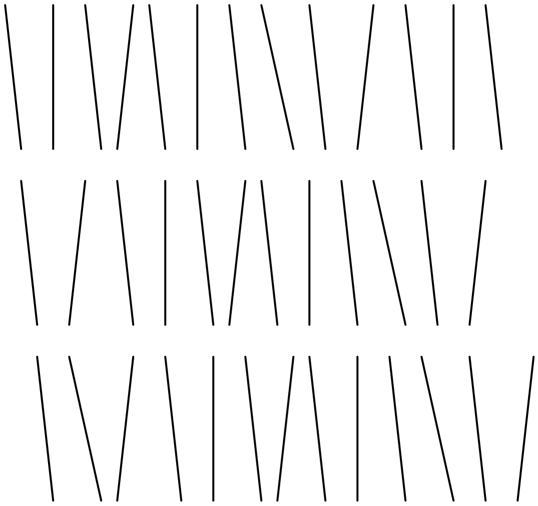

Figure 1.3 Schematic picture of a smectic LC phase.

as a layer structure. Inside the layer structure, the LC molecules behave like a nematic phase with an orientation order but without translational order on the other two dimensions. There are many different types of the smectice phases like smectic A, smectic B etc. The difference in properties of these smectic phases are: (1) the orientation of the preferential director of the molecules inside the layer with respect to the normal of the layer. (orthogonal or tilted to the layer) (2) the organization of the centers of the mass of molecules inside the layers. For a smectic A LC, the molecules form a layer structure with a preferential alignment along a particular direction inside the layer. This preferential direction is parallel to the normal of the layer. Typically, the interlayer distance is 1~2 times of the length of LC molecules. This is clearly an idealization, because x-ray scattering experiments have demonstrated quite convincingly that the variation of the average density along the director is *sinusoidal* in smectics. For example, the incompressible hard core of the cyanide and phenyl group in 4-*n*-octyl-4′-cyanobiphenyl (8CB) forms a high density layer structure while the flexible alkyl chains results in the low density “gap” between the layer as shown in the Figure 1.4. The interlayer distance is 1.4 times the molecular length with the structure.[23]

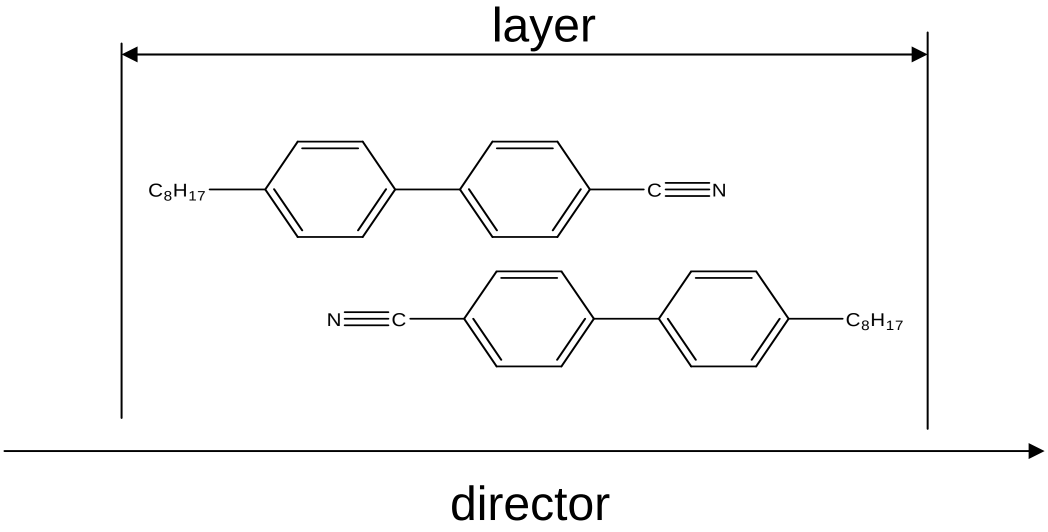

Figure 1.4 Layer Structure of 8CB

1.2.2 ORDER PARAMETER

In order to characterized the orientation order of LCs, two aspects need to be considered: (1) the preferential direction of LC molecules which is called director **n(r)**, and (2) the degree of the ordering i.e. the distribution of the long axis of the molecules with respect to the director. Restricting the discussion to the nematic LC, the average alignment of molecules with their long axis parallel to each other is toward a preferential direction. This direction can be described by a unit-vector which is defined as a nematic director **n(r)**. It is indistinguishable for **n(r)** and – **n(r)** that the polarity of the composite molecules does not cause a macroscopic effect on the nematic phase. The orientation of the nematic director can be controlled either by the symmetry of the substrate or the external field which will be discussed in detail in the next section.

The quantity used to measure the degree of ordering of LC molecules is the order parameter. Imagine that a cluster of rod-like molecules form a nematic phase in space. Microscopically, one can define a unit vector **a(r)** to describe the orientation of the long axis of a rod-like molecule at position r in space. In order to characterize the orientation distribution of the unit vector **a(r)**, a second order tensor which is a traceless symmetry tensor can be written as

$$Q_{i,j} = < a_i a_j > - \frac{1}{3}\delta_{ij}, \qquad i, j = \text{x, y, z} \tag{1-1}$$

Where x, y, z is a lab-fixed frame and δ_{ij} is the Kronecker tensor which equals to 1 when *i=j* and is 0 otherwise. This tensor can be diagonized if choosing a proper coordinate system and can be rewritten as

$$Q_{i,j} = S(n_i n_j - \frac{1}{3}\delta_{ij}), \qquad i, j = \text{x, y, z} \tag{1-2}$$

Where the unit-vector **n** is the director which specifies preferential orientation of the long axes of the LC molecules. S is the scalar order parameter which is the ensemble average of the orientation distribution of the long molecular axis with respect to the nematic director. The order parameter S is defined as

$$\begin{aligned} S &= < \frac{3}{2}\cos^2\alpha - \frac{1}{2} > \\ &= \int (\frac{3}{2}\cos^2\alpha - \frac{1}{2}) f(\alpha) \sin\alpha d\alpha \end{aligned} \tag{1-3}$$

Where α is the angle between the long axis of the rod-like molecule to the nematic director, and f(α) is the distribution function that determines the probability of finding a given orientation of molecule at a given position.

If the orientation of the LC molecules is random, such as the isotropic phase, $< \cos^2 \theta >= \frac{1}{3}$ and S=0. On the other hand, S=1 and $< \cos^2 \theta >= 1$ if the molecules are perfectly aligned which is a character of the crystalline state. The order parameter for a thermotropic liquid crystal is temperature dependent. For example. S of 5CB varies from 0.3~0.4 near the nematic-isotropic transition temperature to ~0.6 at room temperature. The orientations of the molecules are varied from the director, i.e the distribution function of the molecular orientation f(α) in the nematic phase is peaked at 0 or π with a certain peak width. Since the director is indistinguishable from **n(r)** and –**n (r)**, and hence α = 0 and α = π are equivalent, it holds that f(α) = f(π–α). The deviation of α maybe be as large as 40° with an order parameter of 0.4.

1.2.3 THE ALIGNMENT OF THE LIQUID CRYSTAL DIRECTOR

The control of the bulk orientation of the LC molecules in the preferential director plays a critical role in liquid crystal display (LCD) application. In a device the surface induced alignment and the external field perform the alignment of the LC director. The surface morphology leads to different orientations of the LC director. In order to align the LC director parallel to the substrate surface, the polymeric alignment layer which is spin-coated onto the substrate is rubbed unidirectionally. Although the alignment mechanism is under debate, it is widely used in LCD manufacturing. Two major points of view are: (1) the unidirectional rubbing generates periodic microgrooves which might force the first layer of LC molecules on the surface of alignment layer to be parallel to the rubbing direction due to the geometric restriction between the microgroove and the LC molecules.

2) the Van der Waal interactions between the LC molecules and the oriented polymer on the surface of alignment layer. Microscopically, the side chain of the polymer of the alignment layer plays an important role on the Van der Waal interaction. Several groups have synthesized polyimide with different side chains for the alignment layer. After mechanical rubbing, the side chains on the surface of alignment layer have different tilt angle which leads to a pretilt angle of the LC director with respect to the substrate surface. The roughness of the surface also determines the alignment of the LC director, for example, highly rough surfaces, instead of periodic microgroove, cause the alignment of the LC director perpendicular to the surface. Many surface characterization techniques are employed to resolve the mechanism of the surface induced alignment. Optical second harmonic generation (SHG) and sum frequency generation (SFG) vibrational spectroscopy are highly surface sensitive and are used to explore the molecular detail of the polymeric orientation at the surface of the alignment layer. Atomic force microscopy (AFM) is also employed to study the topography of the rubbed surface. Grazing-induced X-ray scattering experiment is applied to determine the rubbing induced orientation of semicrystalline polyimide at the alignment surface.

Applying an external field such as a magnetic or an electric field is an alternative method to align the LC director. Due to the rod-like or disk-like shapes of the molecules, the magnetic susceptibility and dielectric constant between the long axis and short axis of molecules are different. This is known as the magnetic or dielectric anisotropy. For instance, when applying an external electric field exceeding a threshold voltage, the LC molecules start to realign with the direction of the external field. Above the threshold voltage, LC molecules having a dipole moment parallel to the long molecular axis and hence a positive dielectric anisotropy are attracted by the electric field. The opposite case holds for LC molecules with negative dielectric anisotropy. The combination of the surface induced alignment and external field alignment of the LC director is the physical principal of LCD devices. Considering a device composed of LC molecules sandwiched by two transparent electrodes, the unidirectionally rubbed alignment layer leads to a uniform LC director parallel to the substrate. When applying an external electric field above threshold voltage orthogonal to the surface, the LC molecules realign with the electric field due to the dielectric anisotropy. This electric field induced reorientation is called Frederick's transition. However, the director orientation inside the device is not homogeneous. The LC director far away from the LC-substrate interface is aligned with the electric field, but molecules near the surface are still parallel to the substrate. The parallel alignment of molecules near the surface is due to the higher anchoring energy (the interaction between the LC molecules and alignment layer) of the alignment layer compared to the energy generated by the external field. The director orientation at the device interface has been measured by many techniques including optical[24-41] or acoustic[42-45] methods, and has been explained by a elastic continuum theory[46,47].

1.3 CONJUGATED POLYMER IN LIQUID CRYSTAL

It is known that rod-like molecules[48], polymers[49], nanoparticles[50], and carbon nanotubes[51] can exist in ordered liquid crystalline phases. In recent studies, conducting polymers[52], biopolymers[53], and multi-wall carbon nanotubes[54] were dissolved in liquid crystalline hosts showing highly orientational alignment. The semiconducting polymer poly[2-methoxy-5((2-ethylhexyl)oxy)-1,4-phenylenevinylene] (MEH-PPV) dissolved in the nematic phase of 4-n-pentyl-4'-cyanobiphenyl (5CB, Figure 1.5) was found to be almost perfectly aligned with the nematic director[52]. Much larger semi-flexible polymers with contour lengths several to tens of μms were incorporated in a rod-like *fd* virus host and visualized by fluorescence imaging. The polymers showed a coil-to-rod transition induced by the isotropic-to-nematic phase transition of the liquid crystal solvent[53]. These observations demonstrate that a polymeric solute tends to align with the nematic director of the solvent. This solvent-directed alignment of the polymer chains has been explained by a "cooperative solvation" model.[52,55,56] The polymer molecules, which are about 100 times larger than the LC molecules, experience an effective mean solvation potential from a large number of solvent LC molecules, which "cooperatively" force the polymer to align parallel to the director.

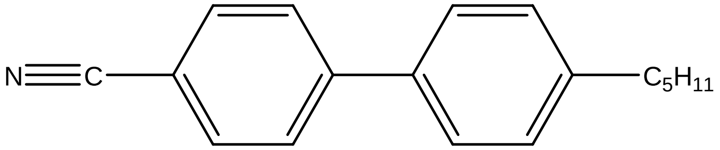

Figure 1.5 Molecular structure of 5CB

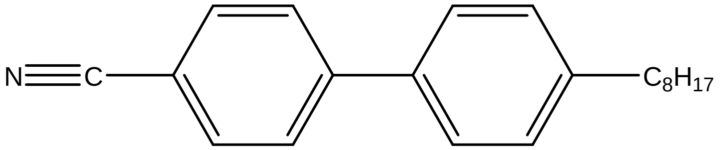

Figure 1.6 Molecular structure of 8CB

This dissertation focuses on studying the structure and dynamics of dilute solutions of conjugated polymer in LC solvent by means of single molecule polarization spectroscopy. Using the unique ability of the single-molecule spectroscopy to study the highly heterogeneous systems, the molecular level information on the influence of the LC solvent on the conformation, orientation and diffusion anisotropy of polymer solute is obtained. A conjugated polymer MEH-PPV is dissolved in the nematic LC solvent 5CB or semectic LC solvent 4-*n*-octyl-4′-cyanobiphenyl (8CB, Figure 1.6). LCs has been in their role as a solvent for the self-assembly of larger host molecules such as polymers. The long-range orientation order in the nematic solvents and special positional order of smectic solvents offers the possibility of fabricating novel nano-structured materials. This dissertation will address several issues of the structure and dynamics of large molecules in such solvents and the dissertation overview will be discussed in the next section.

1.4 DISSERTATION OVERVIEW

The chapters of this dissertation are organized as following.

Chapter 2 describes the experimental method and theoretical background of the data analysis for single molecule polarization spectroscopy to extract information about the conformation and orientation of conjugated polymers in the LC matrix. The experimental method includes the sample preparation, the single molecule polarization spectroscopy to unveil the conformation and orientation of the polymer, and the two beam cross-correlation spectroscopy technique to study the diffusion anisotropy. The theoretical background for the data analysis provides the detailed mathematical formulation for the matlab program to fit the experimental results where the conformation and orientation order of the conjugated polymer are obtained. Finally, the Monte Carlo simulation of a conjugated polymer with different defect concentrations in the LC solvent is also discussed.

Chapter 3 describes the effect of polymer chain segmentation on the ability of nematic solvents to elongate and align polymer chain solutes. Coordinated single molecule spectroscopy and beads-on-a-chain simulations are used to study the orientational and conformational order of a series of segmented conjugated polymers dissolved in the nematic liquid crystal 5CB. The order parameters for alignment and elongation are both observed to decrease with increasing segmentation, reflecting an interplay among conformational entropy, solvation anisotropy, and bending energy of the chain. The elongation of the polymer chain with a variable number of segments measured by single molecule polarization spectroscopy[57] directly reflects the strength of the anisotropic solvation potential over a length scale 10 to 100 times larger than the length of a LC molecule.

Chapter 4 describes the solvation of single conjugated polymer molecules in a smectic liquid crystal using single molecule spectroscopy. The evidence for two distinct orientations for solvation was observed: The majority of polymers are narrowly orientated parallel to the nematic director, as expected, but, unexpectedly, a second population is aligned perpendicular to the director. These molecules reside in the gaps between the layers. This latter type of solvation has not been previously observed and is not expected when the density variation along the director is sinusoidal.

Chapter 5 describes the effects of reorientating LC molecules on the alignment of MEH-PPV by means of single molecule spectroscopy. Using single molecule polarization spectroscopy, we investigated the alignment of a polymer solute with respect to the LC director in a LC device while applying an external electric field. The polymer solute is MEH-PPV and the LC solvent is 5CB. The electric field induces a change in the LC director orientation from a planar alignment (no electric field) to a perpendicular (homeotropic) alignment with an applied field of $5.5*10^3$ V/cm. We find that the polymer chains align with the LC director in both planar and homeotropic alignment when measured in the bulk of the LC solution away from the device interface. Single molecule polarization distributions measured as a function of distance from the LC device interface reveal a continuous change of the MEH-PPV alignment from planar to homeotropic. The observed polarization distributions are modeled using a conventional elastic model that predicts the depth profile of the LC director orientation for the applied electric field. The excellent agreement between experiment and simulations shows that the alignment of MEH-PPV follows the LC director throughout the LC sample. Furthermore, our results suggest that conjugated polymers such as MEH-PPV can be used as sensitive *local* probes to explore complex (and unknown) structures in anisotropic media.

Chapter 6 describes the translational diffusion constant D of a polymer *solute* in a single-domain, nematic liquid crystal *solvent* (5CB), measured in directions parallel and perpendicular to the nematic director, using a fluorescence two-beam, cross-correlation technique. The solute under investigation is the stiff, conjugated polymer, MEH-PPV. The ratio $D_{\|}/D_{\perp}$ of diffusion constants (parallel and perpendicular to the director) is observed to be 1.9 ± 0.3. This is surprisingly small considering that MEH-PPV is known to be both elongated and highly aligned along the liquid crystal director of 5CB. We therefore argue that the structural order parameter of the solvent governs the anisotropy of the diffusion of the solute.

Chapter 2: Methods

2.1 INTRODUCTION

In this chapter, the experimental methods, including the sample preparation, single molecule polarization spectroscopy, fluorescence cross-correlation spectroscopy and electro-optical measurement on the LC device will be described in detail. The theoretical background of the single molecule polarization spectroscopy and the mathematical model for the Matlab program to fit the experimental result are also discussed. In addition, the methodology of Monte Carlo (MC) simulation on the conformation and orientation of single polymer chains in the isotropic and anisotropic medium is explained as well.

2.2 EXPERIMENTAL METHOD

2.2.1 SAMPLE PREPARATION

In this dissertation, MEH-PPV with different conjugated length were used. The synthetic procedure for the MEH-PPV samples with varying conjugation length employs a precursor containing methoxy and acetoxy eliminating groups and has been described in detail previously[58,59]. The structure of MEH-PPV with different conjugated length denoted Mx, where x is the percentage of C=C double bonds is shown in Figure 2.1. We used samples which contained on average 30 and 55 % defects, denoted M70 and M45, respectively. Their average molecular weight M_w was 220,000. The MEH-PPV sample

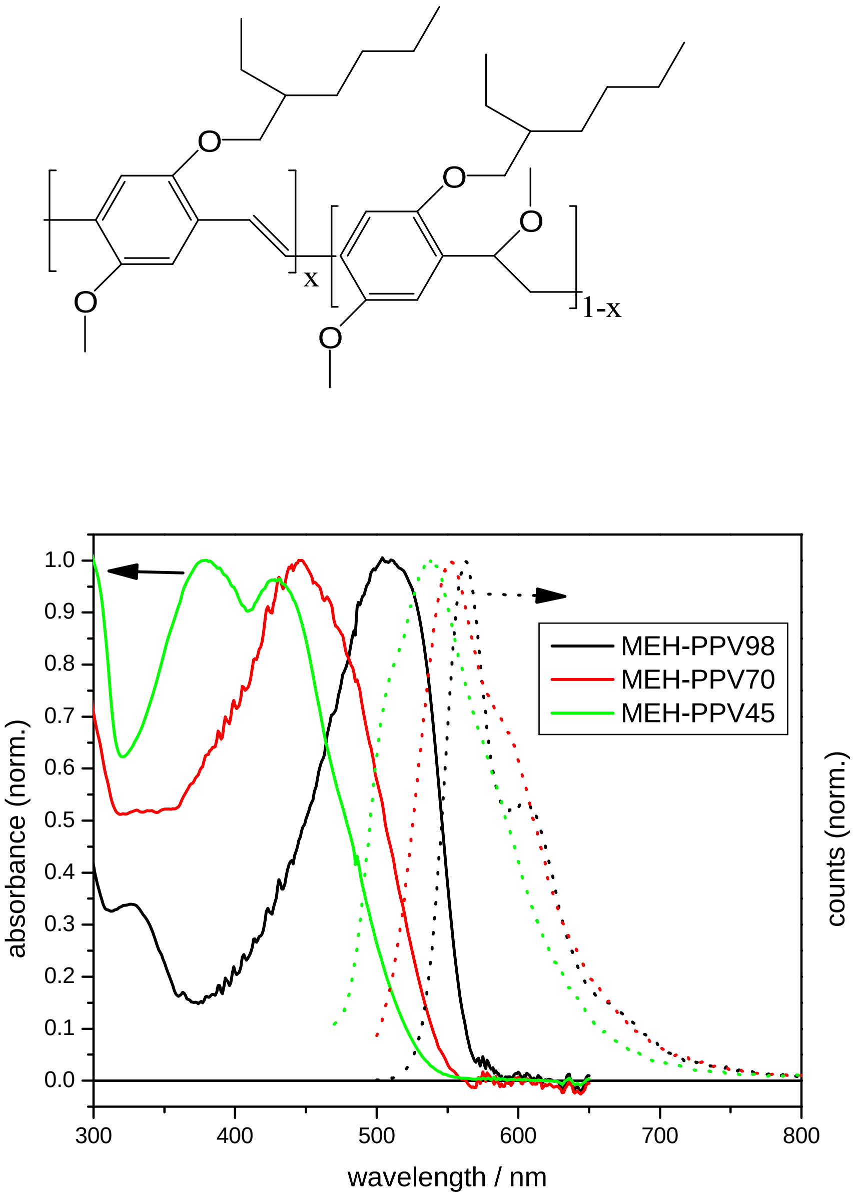

Figure 2.1:Structure of MEH-PPVx, where x is the percentage of C=C double bonds, and absorption and emission spectra of MEH-PPV98, MEH-PPV70, and MEH-PPV45. The excitation wavelengths were 457 nm (MEH-PPV45) and 488 nm (MEH- PPV99 and MEH-PPV70).

without any added defects had an average molecular weight of 110,000 and its synthesis and characterization has been reported as well. This sample showed an absorption maximum at 503 nm in chloroform and we therefore estimated the presence of about 2 % single-bond defects and denote the sample here as M98. In this dissertation, MEH-PPV is referred to M98 if there is no specific notification. Ensemble absorption and emission spectra of all samples are also shown in Figure 2.1. As the conjugation length increases the absorption and emission maxima shift to lower energies because of the larger electron delocalization and a smaller HOMO-LUMO gap. The excitation wavelengths for the emission spectra were 457 nm (MEH-PPV45) and 488 nm (MEH- PPV98 and MEH-PPV70).

Nematic liquid crystal films of MEH-PPV-doped 5CB (Aldrich) with a concentration of 10^{-5}-10^{-8} % by weight were prepared starting from a polymer-5CB-chlorobenzene triphase system, as described previously[52,60]. After evaporation of the chlorobenzene, a drop of the MEH-PPV-5CB mixture was sandwiched between the unidirectionally rubbed PVA alignment layers of a quartz slide and a glass coverslip separated by a 50 μm Mylar spacer. The formation of the nematic liquid crystalline phase was checked by the observation of birefringence under a microscope with crossed polarizers (Zeiss Axioskop 2 Mat).

The smectic LC cell in chapter 4 was made by similar procedure as nematic sample. The cell is composed of regular cover slip and an ITO coated quartz slide with two copper wires. The MEH-PPV-8CB mixture was heated to the temperature at isotropic phase and filled in the cell by the capillary method. The cell was cool down to the room temperature with t cool rate of 1°C/min. At the room temperature, the 8CB is in the smectic phase. The temperature control of the sample during the single molecules measurement was performed by the electric heating on the ITO coated quartz slide and on the objective on the microscope.

The LC device in chapter 5 was made by two ITO coated glass separated by a 12.7 µm Mylar spacer. The MEH-PPV-5CB mixture was filled in the device by capillary action. The electric field (AC, sinusoidal wave with frequency of 1 kHz).was applied perpendicular to the substrate with amplitude of $5.5*10^3$ V/cm (RMS voltage) while performing the single molecule measurement. The LC device was characterized by the electro-optical measurement.

Electro-optical measurements are performed by using an incident laser beam of 488 nm passing through a front polarizer, then a nematic cell, followed by a rear polarizer (i.e. analyzer). The signal *I(V)* is detected by an avalanche photo diode (APD, Perkin-Elmer SPCM), as shown in Figure 2.2. The analyzer and the nematic director of the LC are orientated 90° and 45° with respect to the front polarizer, respectively. The transmittance is measured as a function of applied electric field (AC, sinusoidal wave with frequency of 1 kHz).

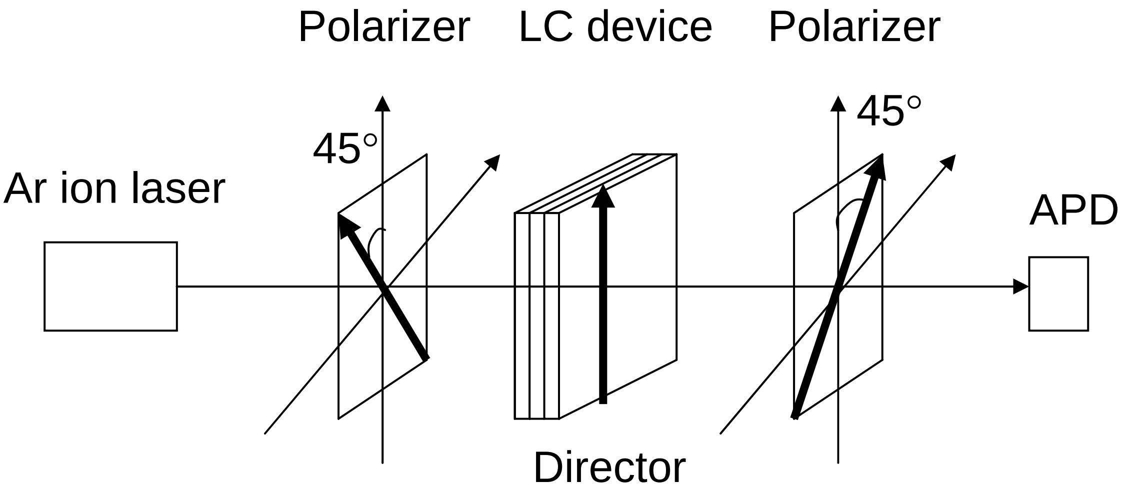

Figure 2.2 Experimental setup for the electro-optical measurements.

2.2.2 SINGLE MOLECULE POLARIZATION SPECTROSCOPY

Single molecule polarization experiments were performed on a home-built confocal microscope consisting of a conventional inverted microscope (Zeiss Axiovert 200), a continuous-wave (cw) ArKr ion laser (LaserPhysics), and two photon-counting avalanche photodiodes (APD, Perkin-Elmer SPCM)) as shown in Figure 2.3. Dual channel data acquisition of fluorescence bursts was accomplished with a commercially available photon counter/multiscaler (Becker&Hickl PMS-400). The liquid crystal samples were mounted on a manual rotation and x-y translation stage with the coverslip facing a 100X oil immersion objective (Zeiss Fluar, Numerical Aperture (NA) = 1.3). The rotation stage allowed for convenient 360 degrees sample rotation while the translation stage enabled us to shift the laser spot to different regions/domains of liquid crystal. For the emission polarization experiments, the samples were excited with circularly polarized light at 488 nm or 457 nm and the average power was about 100-200 nW which corresponds to 200-400 Wcm^{-2} assuming a diffraction-limited laser spot size of 250 nm. The emission bursts were collected by the same objective and were filtered by a notch and long-pass filter in order to remove scattered laser light. Using a polarizing cube beamsplitter the x- and y-components of the polarized emission (I_x and I_y) are detected by the two APDs. Our setup is such that the x- and y-components are in the plane of the liquid crystal sample with the exciting laser light propagating in the z-direction. The bulk liquid crystal director, n, makes an angle γ with respect to the y-axis and measurements were performed for $\gamma = 0$, $\pi/4$ and $\pi/2$. Typical dual-channel intensity

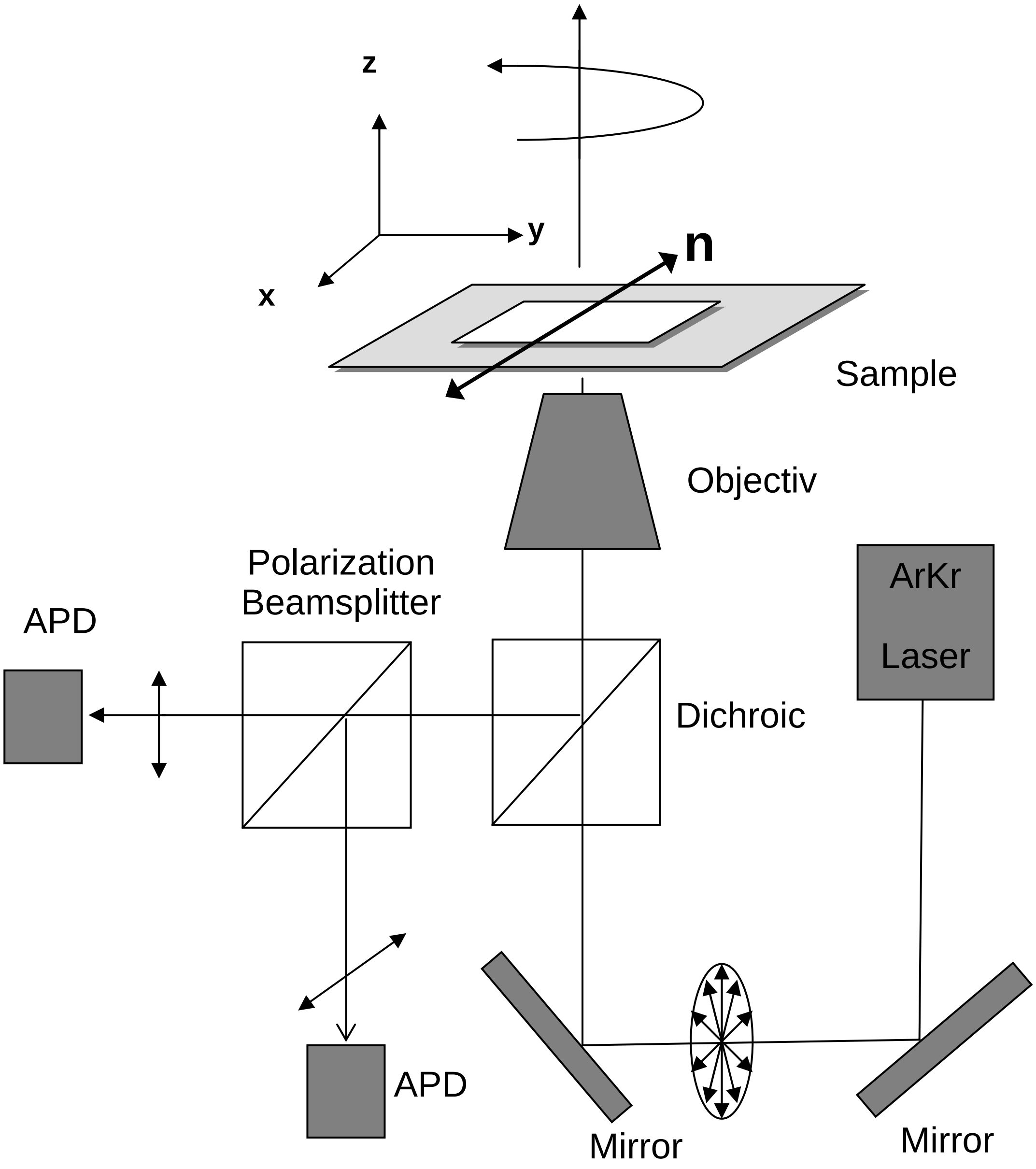

Figure 2.3 xperimental setup a confocal microscope

trajectories for M98 (A), M70 (B), and M45 (C) are shown in Figure 2.4.

Histograms of single-molecule polarizations were generated using an automated routine. Dual channel fluorescence trajectories were acquired for 30 – 60 minutes for each sample orientation using a 10 ms bin time. Because the average burst time was about 50 ms, the data was binned into 50 ms time intervals to create single intensity bursts. After background correction, all points below a threshold value were deleted. The threshold intensity to identify a fluorescence burst was set to three times of the mean background. Due to the intensity threshold, the measurement was biased towards larger polymers and those traveling through the center of the excitation spot. The polarization ratio, *P*, was calculated for each fluorescence burst and therefore one molecule at a time according to:

$$P = \frac{I_y - I_x}{I_y + I_x} \tag{2-1}$$

Polarization histograms were then generated consisting of several hundred fluorescence bursts for each measurement depending on the concentration of the sample and total acquisition time.

For the excitation polarization measurements, two laser beams, one from the ArKr ion laser and a second one from an Ar ion laser (Melles Griot) were focused by the same objective into the liquid crystal sample just above the coverslip. The two excitation beams were linearly polarized along and perpendicular to the liquid crystal nematic director. Their intensities were modulated with opposite phase using two acousto-optic

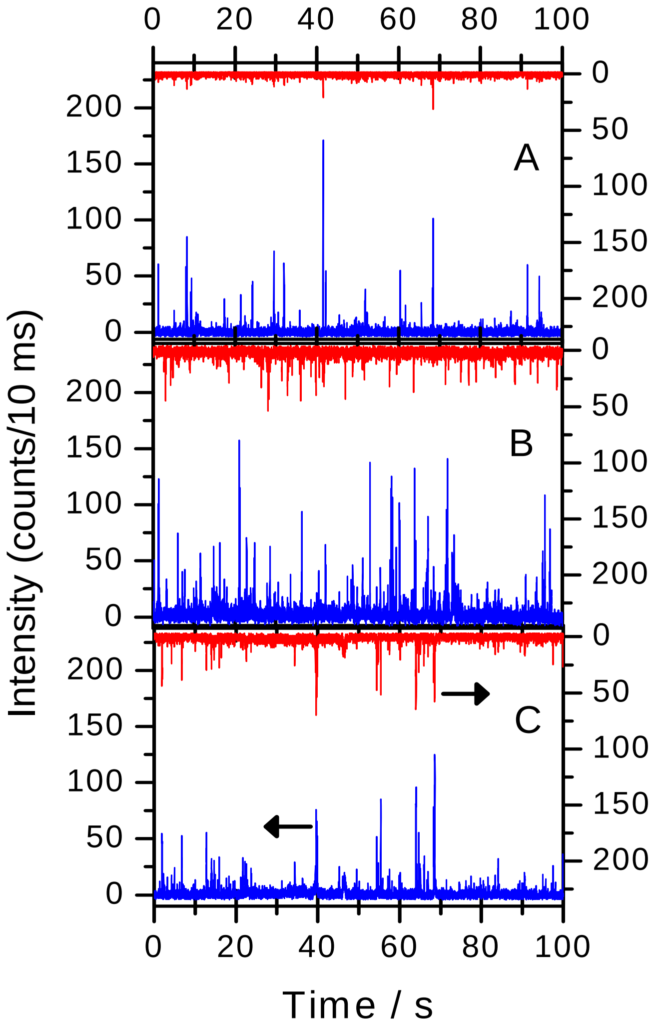

Figure 2.4 Typical dual-channel intensity trajectories for M98 (A), M70 (B), and M45 (C). The fluorescence signal was acquired under cw laser excitation with circularly polarized light at wavelengths of 457 nm (M45) and 488 nm (M98 and M70).

modulators (IntraAction Corp. AOM 403R) controlled by a Hewlett-Packard 8013B pulse generator. The total fluorescence was collected using only one APD. The APD output was split into the two counter board channels which were synchronously gated with the laser modulation. The modulation frequency was chosen to be 100 times larger than the bin time (10 ms). The excitation polarization was calculated according to equation (2-1) where I_x and I_y corresponds to excitation perpendicular and parallel to the director, *n*.

2.2.3 THEORETICAL BACKGROUND OF DATA ANALYSIS FOR SINGLE MOLECULE POLARIZATION SPECTROSCOPY

In this section, the theoretical background of the single molecule polarization measurement of the conjugated polymer in LC matrix will be discussed as following, (1) how the order parameter in a LC is the defined, (2) how bulk measurements are used to determine the static orientational order parameter of single dipoles, (3) how single molecule polarization spectroscopy can be used to determine the orientational order parameter as well as the intrinsic molecular anisotropy of a polymer, and (4) how depolarization effects have to be included.

In an uniaxial LC, the orientational order of the molecules can be described by a normalized probability distribution function f(α), which only depends on the angle, α, between the long molecular axis and the major axis of the system known as the (nematic) director. It is common to expand f(α) by even Legendre polynomials $P_l(\cos\alpha)$, where the moments of the distribution are[61]:

$$< P_l(\cos\alpha) > \equiv < P_l > = \int_0^{\pi} f(\alpha) P_l(\cos\alpha) \sin\alpha d\alpha \qquad (2\text{-}2)$$

The order parameter of the system is given by the first nontrivial term, which is $S = < P_2(\cos\alpha) > = < \frac{3}{2}\cos^2\alpha - \frac{1}{2} >$[61]. The order parameter is an indicator for the orientational order of the molecules, where S = 1 presents perfect and S = 0 random alignment of the molecules.

Absorption and fluorescence anisotropy measurements have been employed to determine the order parameter of fluorescent probe molecules dissolved in an uniaxial liquid crystal. The shape and size of the probe molecule is usually chosen as to resemble the liquid crystal molecules. The absorption anisotropy is defined as $r_A = \frac{A_{//} - A_{\perp}}{A_{//} + 2A_{\perp}}$[60], where $A_{//}$ and $A_{\perp}$ are the absorbance measured with polarized excitation light parallel and perpendicular to the major axis of the liquid crystal, respectively. The order parameter of the probe molecules and hence the liquid crystal can be calculated through the following equation[60,62]:

$$S_A = r_A \frac{2}{3\cos^2\zeta - 1} \tag{2-3}$$

where ζ is the angle between the absorption transition dipole and the long axis of the molecule.

Similarly, the order parameter can also be obtained from the fluorescence anisotropy according to[60,62]:

$$S_F = r_F \frac{2}{3\cos^2\zeta' - 1} \tag{2-4}$$

with

$$S_F = \frac{I_{//} - I_{\perp}}{I_{//} + 2I_{\perp}} \tag{2-5}$$

where $I_{//}$ and $I_{\perp}$ are the fluorescence intensities polarized parallel and perpendicular to the nematic director and ζ' is the angle between the emission transition dipole and the long axis of the molecule. Fluorescence anisotropy studies on liquid crystals are usually performed with unpolarized excitation light because of the aligned nature of the sample.

Absorption and fluorescence anisotropy measurements can determine the static order parameter of simple molecules with well defined transition dipoles. In order to extract more complex information about the relative orientation of the absorption and emission dipoles and the rotational diffusion of the molecules, photoselection experiments, absorption dichroic ratio measurements, and time dependent polarization experiment are employed[61,63,64]. For ensemble measurements one always obtains the average values of the measured properties. On the other hand, single molecule studies are a powerful complementary technique which allows one to measure distributions directly. Single molecule spectroscopy can simultaneously explore the static orientation but also the dynamics of molecules. Polarization modulation and fluorescence polarization measurements have been employed to investigate the conformation of macromolecules labeled with a single chromophoric dye as well as rotational dynamics[65,66]. In order to study the orientation of a conjugated polymer, an intrinsically multichromophoric system, it is necessary to understand the conformation of the polymer as well as the orientational alignment of the polymer with respect to the nematic director. Single molecule polarization measurements are a powerful method to extract this information.

In our experiment, the excitation and fluorescence polarization measurements were performed on MEH-PPV, which is dissolved in the nematic liquid crystal 5CB. A single MEH-PPV polymer chain contains several hundred chromophores where each chromophore consists of 10~15 repeat units[67]. Each polymer therefore presents an ensemble of individual chromophores or segments. In the excitation experiment, the measured fluorescence intensity is proportional to $\sum_i \left|\vec{\mu}_i \cdot \vec{E}\right|^2$, where $\vec{\mu}_i$ is the transition dipole of segment i and $\vec{E}$ is the electric field of the excitation light. In order to connect the excitation polarization to a molecular property, it is convenient to define a molecular anisotropy, A, within a molecular dependent frame x', y', z' according to:

$$A = \frac{\sum_i \mu_{ix'}^2 - \frac{1}{2}\sum_i \mu_{iy'}^2 + \mu_{iz'}^2}{\sum_i \mu_{ix'}^2 + \frac{1}{2}\sum_i \mu_{iy'}^2 + \mu_{iz'}^2} \qquad (2\text{-}6)$$

where $\mu_{ix'}$ is the transition dipole of the i^th^ segment projected onto the major optical axis of the polymer (x' axis). In analogy to the external orientational order parameter for the alignment of molecules in an uniaxial host, we can define an internal bond order parameter of the polymer as $s = < \frac{3}{2}\cos^2\beta - \frac{1}{2} >$, where β is the angle between a segment and x'. It is straightforward to show that the relationship between the molecular anisotropy and the internal bond order parameter is $A = \frac{3s}{2+s}$, assuming each segment length is the same.

The experimentally measured polarization is deconvoluted into two contributions arising from the orientational alignment and the intrinsic molecular anisotropy of the polymers. This system is therefore more complicated to analyze compared to the alignment of single dipoles due to the distribution of intrinsic molecular anisotropies, A. In order to extract the orientational order of the polymer in the liquid crystal, the orientational distribution function is required. It is straightforward to express the orientational distribution function through a Boltzmann distribution according to:

$$f(\alpha) = \frac{e^{-V(\alpha)/kT}}{\int_0^{\pi} e^{-V(\alpha)/kT} \sin\alpha d\alpha} \qquad (2\text{-}7)$$

where $V(\alpha)$ is the mean potential $V(\alpha) = -\nu\langle P_2(\cos\alpha)\rangle P_2(\cos\alpha)$ with an intermolecular interaction strength ν[68] Considering the propagation of polarized light through a high NA objective[69,70], the polarization of the emission can be written as a function of A, α, η, according to (see appendix A),

$$P = \frac{I_y - I_x}{I_y + I_x} = \frac{-(C_1 - C_2)A(\cos^2\alpha - \sin^2\alpha\cos^2\eta)}{A[(2C_3 - C_1 - C_2)\sin^2\alpha\sin^2\eta - C_3] + (C_1 + C_2 + C_3)} \text{ at } \gamma = 0 \qquad (2\text{-}8)$$

$$P = \frac{I_y - I_x}{I_y + I_x} = \frac{2(C_1 - C_2)A\cos\alpha\sin\alpha\cos\eta}{A[(2C_3 - C_1 - C_2)\sin^2\alpha\sin^2\eta - C_3] + (C_1 + C_2 + C_3)} \text{ at } \gamma = \pi/4 (2\text{-}9)$$

where α, η are the polar angle and azimuthal angle with respect to the nematic director and the axis perpendicular to the nematic director, respectively. The coefficients C_1, C_2, C_3 are microscope objective correction factors.

The probability distribution function for the polarization is obtained by assuming a Gaussian distribution for the molecular anisotropy, f(A), according to:

$$f(A)=\frac{1}{\sqrt{2\pi\sigma_A^2}}e^{-\frac{(A-\overline{A})^2}{2\sigma_A^2}} \tag{2-10}$$

$\overline{A}$, and σ_A are the mean and standard deviation of the molecular anisotropy. The final polarization histogram can be obtained by computing the total probability distribution function, f(A)*f(α), and integrating over all orientations given by the polar and azimuthal angle, α and η. Therefore, both the intrinsic molecular anisotropy and orientational distribution are determined through the measured polarization distributions at $\gamma = 0$ and $\pi/4$.

Fluorescence depolarization is known to contain information about the dynamics of chromophores in solution and, in addition, to influence the fluorescence anisotropy[71,72]. Three depolarization effects are discussed, which result from (1) intrachain energy transfer in the polymer, (2) rotational diffusion or wobbling of the polymer and (3) birefringence of the liquid crystal.

Interchain and intrachain energy transfer occur in polymers during the fluorescence relaxation time after photoexcitation[71]. The energy transfer is dependent on the concentration and conformation of the polymer[10,60,71,73]. However, intrachain energy transfer is dominant if the polymer concentration is very low in solution[73], which is the case in our experiment. The mechanisms of intrachain energy transfer are exciton hopping along the main polymer chain or Forster energy transfer through space. Both mechanisms result in the transfer of the excitation energy to the lowest energy or defect site[10]. It is known that the hopping process is much slower than the Forster process[73]. Hence, the Forster process dominates if both processes exist. In the Forster process, the energy transfer rate depends on the distance and orientation of two adjacent dipoles. As a result, the efficiency of the energy transfer is related to the conformation of the polymer. If the polymer is extended, the hopping process is important because the chromophores are far away from each other. On the other hand, if the polymer is collapsed, the chains are close to each other, which leads to energy funneling to the lowest energy site due to the fast Forster energy transfer. Both hopping and Forster energy transfer can lead to different orientations between the initial absorption and final emission dipole, and hence change the observed fluorescence anisotropy.

Rotational diffusion or wobbling of molecules is another depolarization effect. Time-resolved fluorescence anisotropy measurements are usually employed to extract this information[63,64,72,74,75]. The fluorescence anisotropy decay relies upon the interplay between the wobbling rate compared to the fluorescence lifetime of the chromophore. If the wobbling is much faster than the fluorescence relaxation (fast wobbling), the emission dipole loses any 'memory' about the excitation. Hence, the emission polarization is independent on the excitation polarization. In contrast, if the time scale of wobbling is much longer than the fluorescence lifetime but shorter than the measurement time (slow wobbling), the dipole appears 'static' within the fluorescence life time, but rotates during the acquisition time. The wobbling of molecules therefore reduces the measured polarization anisotropy.

Photoselection experiments have been employed to examine the wobbling. The general equation of polarized fluorescence intensity considering wobbling can be written as[70]:

$$ {}_{\varepsilon}I_{\varsigma} = K\int_0^\infty \iint \rho(\theta_a,\phi_a,\theta_e,\phi_e,t)\frac{1}{\tau}e^{-\frac{t}{\tau}}P_a(\theta_a,\phi_a,\hat{\varepsilon})P_e(\theta_e,\phi_e,\hat{\varsigma})d\Omega_a d\Omega_e dt \qquad \text{(2-11)} $$

where ρ is the correlation function of finding the absorption dipole at orientation $(\theta_{a,}\phi_a)$ and the emission dipole at orientation $(\theta_{e,}\phi_e)$ after some delay time, t. $P_{a,(e)}$ is the absorption (emission) probability due to an absorption (emission) dipole at orientation $(\theta_{a,}\phi_a)$ $((\theta_{e,}\phi_e))$ with excitation (emission) polarization $\hat{\varepsilon}$ ($\hat{\varsigma}$). $d\Omega_a = \sin\theta_a d\theta_a d\phi_a$ and $d\Omega_e = \sin\theta_e d\theta_e d\phi_e$. The intensity is integrated for all orientations of absorption and emission dipoles over all time. For fast wobbling, the emission dipole does not correlate with the absorption dipole, and we can express the polarized fluorescence intensity as:

$$ {}_{\varepsilon}I_{\varsigma} = K\int \rho_a(\theta_a,\phi_a)P_a(\theta_a,\phi_a,\hat{\varepsilon})d\Omega_a \int \rho_e(\theta_e,\phi_e)P_e(\theta_e,\phi_e,\hat{\varsigma})d\Omega_e \qquad \text{(2-12)} $$

Where $\rho_a(\theta_a,\phi_a)$ and $\rho_e(\theta_e,\phi_e)$ are the time independent probability of finding the absorption and emission dipole from $\rho(\theta_a,\phi_a,\theta_e,\phi_e,t)$. Therefore, the polarization anisotropy can be written according to:

$$ P = \frac{{}_xI_y - {}_xI_y}{{}_xI_y + {}_xI_y} = \frac{\int \rho_e(\theta_e,\phi_e)(P_e(\theta_e,\phi_e,\hat{y}) - P_e(\theta_e,\phi_e,\hat{x}))d\Omega_e}{\int \rho_e(\theta_e,\phi_e)(P_e(\theta_e,\phi_e,\hat{y}) + P_e(\theta_e,\phi_e,\hat{x}))d\Omega_e} \qquad \text{(2-13)} $$

Notice that the polarization for the fast wobbling is independent on the excitation polarization. This reduces the polarization anisotropy because the dipole is not well aligned along a certain direction if taking fast wobbling into account.

In the slow wobbling case, the absorption and emission dipoles are 'static' ρ becomes time independent. Hence, we can calculate the polarization through the following equation:

$$P = \frac{{}_xI_y - {}_xI_y}{{}_xI_y + {}_xI_y} = \frac{\iint \rho(\theta_a,\phi_a,\theta_e,\phi_e) P_a(\theta_a,\phi_a,\hat{x})(P_e(\theta_e,\phi_e,\hat{y}) - P_e(\theta_e,\phi_e,\hat{x})) d\Omega_a d\Omega_e}{\iint \rho(\theta_a,\phi_a,\theta_e,\phi_e) P_a(\theta_a,\phi_a,\hat{x})(P_e(\theta_e,\phi_e,\hat{y}) + P_e(\theta_e,\phi_e,\hat{x})) d\Omega_a d\Omega_e} \quad (2\text{-}14)$$

Note that the integration of over $d\Omega_a$ and $d\Omega_e$ are not separable. Because the measuring time is longer than the wobbling time, the molecule is excited continuously while it is wobbling during the measurement. As a result, the polarization is reduced because the molecule is rotating back and forth.

It is well known that the polarization state of light is changed if linearly polarized light passes through a birefringence material[76,77]. Consequently, the depolarization effect due to the birefringence should be considered if performing optical measurements with linearly polarized light on a birefringence material, such as a liquid crystal device[76,78]. In the single molecule measurement, the experiment is performed through an objective with a high NA, which causes an additional depolarization effect[69]. This problem is addressed by the microscope correction factors which depend on the NA of the objective and the refractive index of the sample[69,70]. However, the microscope correction factors are also related to the birefringence of the liquid crystal device. We developed a model to calculate the microscope correction factors from a fluorescent emitter in an uniaxial liquid crystal (appendix B). In this model, a fluorescent emitter located at a specific physical depth in the liquid crystal is excited by circularly polarized light. Then it emits polarized (monochromatic) fluorescence parallel to the emission dipole and towards the objective. It is assumed that there is no refraction and reflection at the interface of the glass substrate and the liquid crystal. As a result, the microscope correction factors vary with physical depth tremendously at $\gamma = \pi/4$, while they are only slightly dependent on physical depth at $\gamma=0$. The polarization anisotropy changes with the physical depth because the measured polarization is related to the microscope correction factors according to equation (2-8) and (2-9).

2.2.4 TWO BEAM FLUORESCENCE CROSS-CORRELATION SPECTROSCOPY

The fluorescence cross-correlation experiments are performed on a home-built confocal microscope (Figure 2.5) with two independent focal volumes/detector system channels. The apparatus is based on an inverted microscope (Zeiss Axiovert 200). Two laser beams are focused by the same objective (Zeiss Fluar, 100X, N.A. = 1.3) forming two independent diffraction limited focal volumes in the nematic LC sample, a few microns above the coverslip. Independent continuous-wave ion laser sources are employed for the two respective focal volumes to remove spurious cross-correlations signals due to laser intensity fluctuations. The in focal plane separation distance of the focal volumes is variable in the range of 0-5 μm with a precision of 0.2 μm. The fluorescence from each laser focal volume is collected by the same objective, filtered by a dichroic and a bandpass filter, and independently imaged onto two separate detectors (APD, Perkin-Elmer SPCM). The 50/50 beamsplitter between the body of the microscope and the detectors is used simply for alignment convenience, and both replicas from the beamsplitter each produce two focal spots, but only one is focused on its respective detector. Confocal “spatial filtering” conditions for collection of the

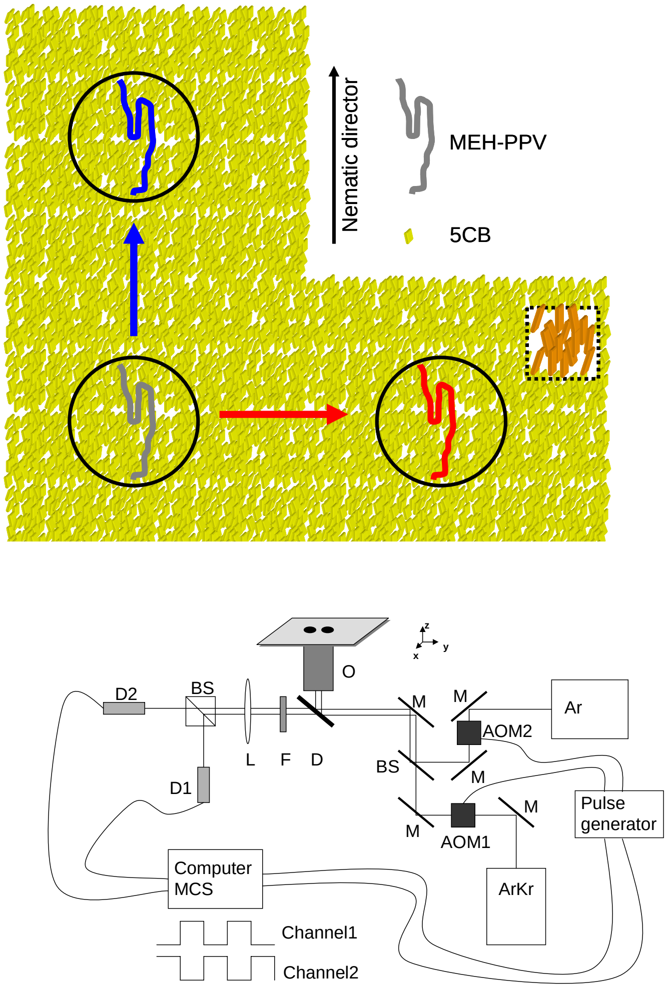

Figure 2.5 Schematic illustration (top) and experimental realization (bottom) of the two-beam cross-correlation setup. M: mirror; AOM: Acousto-optic modulator; BS: 50/50 beamsplitter; D: dichroic; O: objective, F: filter; L: lens; D: detector; MCS: multi-channel scaler.

fluorescence light originating from each of the two laser spots is achieved by using a total image magnification of 850X at the APD detectors (which have an active area of 175 μm). Confocal conditions for detection are necessary in this experiment to narrow the spatial resolution for the diffusion measurements. The LC samples are mounted on a rotation stage allowing for convenient alignment of the director with respect to the direction of the displacement of the two focal volumes.

To remove fluorescence intensity cross-talk between the focal volumes, i.e. detection of fluorescence from the "wrong" focal volume, the two excitation beams are chopped with opposite phase, using two acousto-optic modulators (IntraAction Corp. AOM 403R). The APD outputs are synchronously gated at the input of the counter board (Becker&Hickl PMS-400). The modulation frequency is chosen to be 100 times larger than the bin time (10 ms). Thus, the setup is functionally equivalent to two independent confocal microscopes where each one monitors a different region of the sample separated by only a few microns (Figure 2.5).

2.3 MONTE CARLO SIMULATION

MC simulations were performed using the bond fluctuation method[79], which has been applied to simulating polymer conformations before and was described in detail elsewhere[7]. We used 100 beads on a polymer chain and included different numbers of defects to generate an ensemble of conformations. The simulations further considered intersegment attraction, stiffness of the polymer chain, and a liquid crystal solvation energy. Each bead in the chain presents 2.5 repeat units which corresponds to length of about 1.5 nm. The intersegment interaction was modeled by a Lennard-Jones-like attraction potential between a pair of beads with a depth of E_{cc} according to:

$$\begin{cases} E_{LJ} = \infty & \text{if } l \le 2.1\text{nm} \\ E_{LJ} = 4E_{cc}((\frac{2.1}{l})^{12} - (\frac{2.1}{l})^{6}) & \text{if } 2.1\text{nm} < l \le 4.2\text{nm} \\ E_{LJ} = 0 & \text{if } l > 4.2\text{nm} \end{cases} \qquad (2\text{-}15)$$

where $E_{cc} = 0.6$ kT. Collapsed (poor solvent) and extended (good solvent) conformations were generated with and without intersegment interaction. The chain bending energy was set as $E_{bend} \sim 10\ \text{kTrad}^{-2} * \psi^2$, where ψ is the difference from the equilibrium bond angle (0° for a double bond and 109° for a single bond corresponding to a tetrahedral defect). The liquid crystal solvation energy was modeled as $E_{solv} = E_{LC} * (\cos\alpha)^2$ per segment, where α is the orientation angle of the segment with respect to the liquid crystal director. E_{LC} was chosen to be 1 kT in the MC simulations. The location and the number of defect were varied for these simulation conditions.

2.4 APPENDIX

2.4.1 APPENDIX A: EMISSION POLARIZATION OF A CONJUGATED POLYMER INSIDE A LC MATRIX

The polymer molecule is described in a molecular coordinate system $(\hat{x}', \hat{y}', \hat{z}')$ with components $(\hat{\mu}_1, \hat{\mu}_2, \hat{\mu}_3)$ of the absorption dipole moment, where $|\hat{\mu}_1| \geq |\hat{\mu}_2| \geq |\hat{\mu}_3|$. Let us define an orthogonal coordinate system $(\widehat{e}, \widehat{o}, \widehat{k})$, where $\widehat{e}$ is parallel to the nematic director of the liquid crystal, and $\widehat{z}$ is the direction of light propagation in the image space (see Figure 2.6). Let $\hat{\mu}_1$ make a polar angle, α, to $\widehat{e}$ and an azumuthal angle, η, to $\widehat{o}$ as shown in Figure 2.6. Assuming the polymer as an overall cylindrical shape, $|\hat{\mu}_1| > |\hat{\mu}_2| = |\hat{\mu}_3|$, we can write $\hat{x}'$, $\hat{y}'$ and $\hat{z}'$ as:

$$\begin{aligned}
\hat{x}' &= \cos\alpha\widehat{e} + \sin\alpha\cos\eta\widehat{o} + \sin\alpha\sin\eta\widehat{z} \\
\hat{y}' &= -\sin\alpha\widehat{e} + \cos\alpha\cos\eta\widehat{o} + \cos\alpha\sin\eta\widehat{z} \\
\hat{z}' &= \sin\eta\widehat{o} - \cos\eta\widehat{z}
\end{aligned} \qquad \text{(A2-1)}$$

The projection of $(\hat{\mu}_1, \hat{\mu}_2, \hat{\mu}_3)$ on $(\widehat{e}, \widehat{o}, \widehat{k})$ can be written as e, o, k. Within the random dipole approximation, we can present e^2, o^2 and k^2 acoording to:

$$\begin{aligned}
e^2 &= |\hat{\mu}_1|^2 \cos^2\alpha + |\hat{\mu}_2|^2 \sin^2\alpha; \\
o^2 &= |\hat{\mu}_1|^2 \sin^2\alpha\cos^2\beta + |\hat{\mu}_2|^2 \cos^2\alpha\cos^2\beta + |\hat{\mu}_3|^2 \sin^2\beta; \\
z^2 &= |\hat{\mu}_1|^2 \sin^2\alpha\sin^2\beta + |\hat{\mu}_2|^2 \cos^2\alpha\sin^2\beta + |\hat{\mu}_3|^2 \cos^2\beta;
\end{aligned} \qquad \text{(A2-2)}$$

For γ = 0, i.e $\hat{y} // \widehat{e}, \hat{x} // \widehat{o}$, we can write the emission polarization as:

$$P = \frac{I_y - I_x}{I_y + I_x} = \frac{-(C_1 - C_2)A(\cos^2\alpha - \sin^2\alpha\cos^2\eta)}{A[(2C_3 - C_1 - C_2)\sin^2\alpha\sin^2\eta - C_3] + (C_1 + C_2 + C_3)}; \qquad \text{(A2-3)}$$

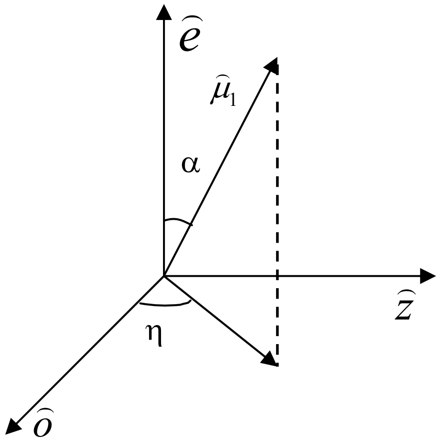

Figure 2.6. Schematic diagram for μ_1 in the $(\widehat{e}, \widehat{o}, \hat{z})$ coordinate. $\widehat{\mu}_1$ has a polar angle, α, to $\widehat{e}$ and an azumuthal angle ,η, to $\widehat{o}$

where A is the molecular anisotropy defined as $A = |\hat{\mu}_1|^2 - |\hat{\mu}_2|^2$. C_1, C_2, C_3 are the microscope correction factors, and the intensities at the two detectors are given by[70]:

$$I_{\hat{x}} = C_1 x^2 + C_2 y^2 + C_3 z^2; \qquad I_{\hat{y}} = C_2 x^2 + C_1 y^2 + C_3 z^2; \tag{A2-4}$$

For $\gamma = \pi/4$, i.e. $\hat{o}$ and $\hat{e}$ both make an angle of 45° with respect to $\hat{x}$ and $\hat{y}$, we can present x and y as:

$$\begin{pmatrix} x \\ y \end{pmatrix} = \begin{pmatrix} \frac{\sqrt{2}}{2} & \frac{\sqrt{2}}{2} \\ -\frac{\sqrt{2}}{2} & \frac{\sqrt{2}}{2} \end{pmatrix} \begin{pmatrix} e \\ o \end{pmatrix}; \tag{A2-5}$$

Therefore, the polarization anisotropy can be written according to:

$$P = \frac{2(C_1 - C_2) A \cos\alpha \sin\alpha \cos\eta}{A[(2C_3 - C_1 - C_2)\sin^2\alpha \sin^2\eta - C_3] + (C_1 + C_2 + C_3)} \tag{A2-6}$$

2.4.2 APPENDIX B: BIREFRIGENCE EFFECT ON THE MICROSCOPY CORRECTION FACTOR

In this appendix we derive the microscopy correction factors taking explicitly the birefringence of the liquid crystal into account. In order to describe the experimental system, we define a lab coordinate system $(\hat{x}, \hat{y}, \hat{z})$ where z is the microscope axis, a non-fixed coordinate system $(\hat{x}'', \hat{y}'', \hat{z}'')$ in the objective space, and a non-fixed coordinate system $(\hat{e}, \hat{o}, \hat{k})$ in the liquid crystal space as shown in Figure 2.7. A dipole emitter is located in an uniaxial birefringence material (liquid crystal) at a physical depth of d μm

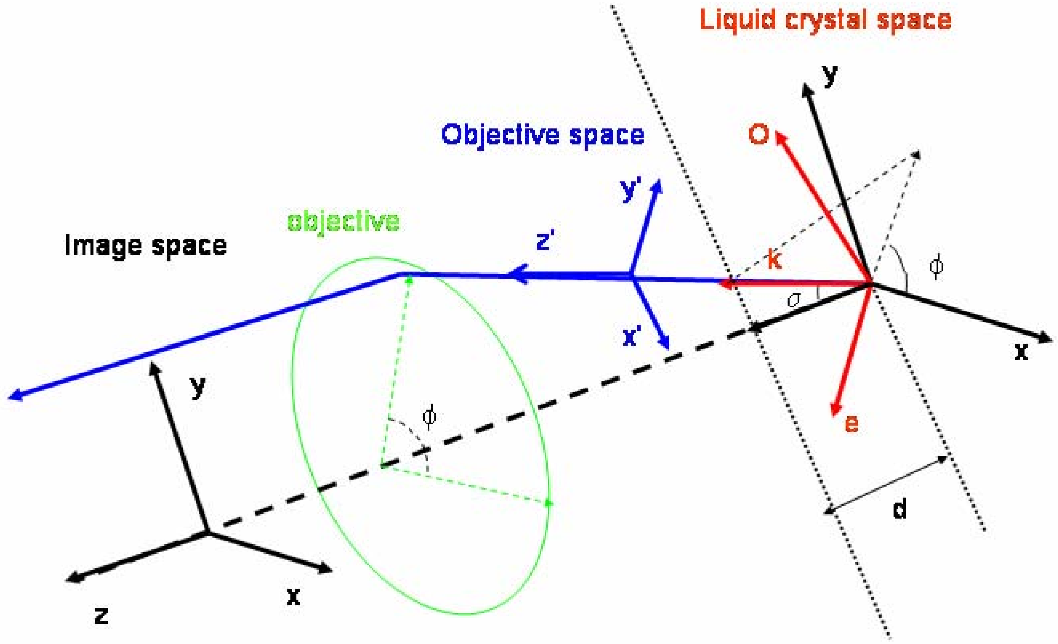

Figure 2.7. A lab coordinate system (x, y, z), a non-fixed coordinate system (x', y', z') in objective space, and a non-fixed coordinate system (e, o, k) in liquid crystal space. A dipole emitter is in the liquid crystal at a physical depth of d micron. The emitted fluorescence propagates towards the objective through the liquid crystal with a polar angle σ to z and azimuthal angle ϕ to x. The fluorescence is collected in image space. The emitted light propagates along z' with polarization parallel to x' in objective space and along z with polarization parallel to x after the objective in image space.

from the interface and is excited by circularly polarized light. It emits monochromatic light with linear polarization parallel to the dipole and an amplitude equal to the dipole strength. The emission propagates through the liquid crystal towards to the objective with a polar angle σ to $\hat{z}$ and azimuthal angle ϕ to $\hat{x}$. The emission is collected in the image space. We assume that the refractive index of the liquid crystal is similar to that of the glass, and thus there is no refraction and reflection at the interface. In accordance with a previous study, light with linear polarization parallel to $\hat{x}"$ ($\hat{y}"$) propagates along $\hat{z}"$ in objective space towards to objective, and then propagates along z with linear polarization parallel to $\hat{x}$ ($\hat{y}$)[69]. The relationship between $(\hat{x},\hat{y},\hat{z})$ and $(\hat{x}",\hat{y}",\hat{z}")$ can be written according to:

$$
\begin{aligned}
\hat{x}" &= (\cos\sigma\cos^2\phi + \sin^2\phi)\hat{x} + (\cos\sigma\cos\phi\sin\phi - \cos\phi\sin\phi)\hat{y} - \sin\sigma\cos\phi\hat{z} \\
\hat{y}" &= (\cos\sigma\cos\phi\sin\phi - \cos\phi\sin\phi)\hat{x} + (\cos\sigma\sin^2\phi + \cos^2\phi)\hat{y} - \sin\sigma\sin\phi\hat{z} \\
\hat{z}" &= \sin\sigma\cos\phi\hat{x} + \sin\sigma\sin\phi\hat{y} + \cos\sigma\hat{z}
\end{aligned}
\qquad \text{(A2-7)}
$$

Thus, the projection of the emission intensity onto $\hat{x}"$ ($\hat{y}"$) in objective space presents the emission intensity with $\hat{x}$ ($\hat{y}$) polarization in the image space. The non-fixed coordinate system $(\hat{e},\hat{o},\hat{k})$ in the liquid crystal space consists of extraordinary and ordinary axis of the liquid crystal and the propagation direction of the emission, respectively. The polarization of the light is usually described by the extraordinary and ordinary axis in the liquid crystal. We calculate the microscope correction factors by expressing the emitter in the lab coordinate system $(\hat{x},\hat{y},\hat{z})$, projecting it onto $(\hat{e},\hat{o},\hat{k})$ in the liquid crystal space, and then projecting it on $(\hat{x}",\hat{y}",\hat{z}")$ in the objective space, which automatically indicates $(\hat{x},\hat{y},\hat{z})$ in the image space.

(a) The nematic director and optical axis of the liquid crystal are parallel to $\hat{x}$ (γ = 0):

Let **c** be the unit vector for the nematic director**.** $\hat{o}$ and $\hat{e}$ can then be obtained via

$$\hat{o} = \frac{\hat{k} \times \hat{c}}{\left|\hat{k} \times \hat{c}\right|} \text{ and } \hat{e} = \frac{\hat{o} \times \hat{k}}{\left|\hat{o} \times \hat{k}\right|}$$

The emission propagates towards the objective in the liquid crystal with a polar angle σ and an azimuthal angle ϕ to $\hat{z}$ and $\hat{x}$, respectively. $\hat{e}$ and $\hat{o}$ can therefore also be written as:

$$\hat{e} = \frac{\cos^2\sigma + \sin^2\sigma\sin^2\phi}{\sqrt{\cos^2\sigma + \sin^2\sigma\sin^2\phi}}\hat{x} - \frac{\sin^2\sigma\sin\phi\cos\phi}{\sqrt{\cos^2\sigma + \sin^2\sigma\sin^2\phi}}\hat{y} - \frac{\sin\sigma\cos\sigma\cos\phi}{\sqrt{\cos^2\sigma + \sin^2\sigma\sin^2\phi}}\hat{z};$$
$$\hat{o} = \frac{\cos\sigma}{\sqrt{\cos^2\sigma + \sin^2\sigma\sin^2\phi}}\hat{y} - \frac{\sin\sigma\sin\phi}{\sqrt{\cos^2\sigma + \sin^2\sigma\sin^2\phi}}\hat{z}$$

(A2-8)

Assuming a transition dipole with a dipole strength on $(\hat{x}, \hat{y}, \hat{z})$ given by x, y, z, we can calculate the emission amplitude parallel to $\hat{x}''$ and $\hat{y}''$ through the liquid crystal in objective space according to:

$$\begin{pmatrix} x' \\ y' \end{pmatrix} = \begin{pmatrix} \hat{x}'\cdot\hat{e} & \hat{x}'\cdot\hat{o} \\ \hat{y}'\cdot\hat{e} & \hat{y}\cdot\hat{o} \end{pmatrix}\begin{pmatrix} e^{i\delta} & 0 \\ 0 & 1 \end{pmatrix}\begin{pmatrix} e \\ o \end{pmatrix}$$
$$= \frac{1}{\cos^2\sigma + \sin^2\sigma\sin^2\phi}\begin{pmatrix} \cos\sigma\cos^2\phi + \sin^2\phi & \cos\phi\sin\phi - \cos\sigma\cos\phi\sin\phi \\ \cos\sigma\cos\phi\sin\phi - \cos\phi\sin\phi & \cos\sigma\cos^2\phi + \sin^2\phi \end{pmatrix}\begin{pmatrix} e^{i\delta} & 0 \\ 0 & 1 \end{pmatrix} \times$$
$$\begin{pmatrix} (\cos^2\sigma + \sin^2\sigma\sin^2\phi)x - \sin^2\sigma\sin\phi\cos\phi y - \sin\sigma\cos\sigma\cos\phi z \\ \cos\sigma y + \sin\sigma\sin\phi z \end{pmatrix}$$

(A2-9)

where $\delta = \frac{2\pi(n_e'-n_o)d}{\lambda\cos\sigma}$, $\frac{1}{n_e'^2} = \frac{\cos^2\sigma}{n_e^2} + \frac{\sin^2\sigma}{n_o^2}$. n_e and n_o are the extraordinary and ordinary refractive index of the liquid crystal, λ is the wavelength of the emission, and d is the physical depth of dipole from interface. $\frac{d}{\cos\sigma}$ presents the optical path.

In the sequence of matrices, the third matrix presents the projection of x, y, z onto $\hat{o}$ and $\hat{e}$. The second matrix presents the phase retardation of the e and o waves in the liquid crystal and the first matrix presents the projection matrix of $(\hat{e},\hat{o})$ to $(\hat{x}',\hat{y}')$. It is assumed that there is no reflection and refraction on the interface of the liquid crystal and the glass substrate.

After multiplying these matrices, one obtains:

$$\begin{aligned}
x' = {} & (\cos\sigma\cos^2\phi + \sin^2\varphi)e^{i\delta}x \\
& +[\frac{(\cos\sigma - \cos^2\sigma)\cos\phi\sin\phi}{\cos^2\sigma + \sin^2\sigma\sin^2\phi}(1-e^{i\delta}) + (\cos\sigma\cos\phi\sin\phi - \cos\phi\sin\phi)e^{i\delta}]y \\
& -[\frac{(1-\cos\sigma)\sin\sigma\cos\phi\sin^2\phi}{\cos^2\sigma + \sin^2\sigma\sin^2\phi}(1-e^{i\delta}) + \sin\sigma\cos\phi e^{i\delta}]z;
\end{aligned} \tag{A2-10}$$

$$\begin{aligned}
y' = {} & (\cos\sigma\sin\phi\cos\phi - \cos\phi\sin\varphi)e^{i\delta}x \\
& +[\frac{\cos^2\sigma\cos^2\phi + \cos\sigma\sin^2\phi}{\cos^2\sigma + \sin^2\sigma\sin^2\phi}(1-e^{i\delta}) + (\cos\sigma\sin^2\phi + \cos^2\phi)e^{i\delta}]y \\
& -[\frac{\cos\sigma\sin\sigma\cos^2\phi\sin\phi + \sin\sigma\sin^3\phi}{\cos^2\sigma + \sin^2\sigma\sin^2\phi}(1-e^{i\delta}) + \sin\sigma\sin\phi e^{i\delta}]z
\end{aligned} \tag{A2-11}$$

Therefore, the emission intensities parallel to x and y in image space, $I_{\hat{x}}, I_{\hat{y}}$, can again be written as:

$$I_{\hat{x},\hat{y}} = \int_0^{\sigma_0} d\sin\sigma \int_0^{2\pi} d\phi (x', y')^2, \tag{A2-12}$$

This gives:

$$\begin{aligned} I_{\hat{x}} &= a_1 x^2 + b_1 y^2 + c_1 z^2; \\ I_{\hat{y}} &= a_2 x^2 + b_2 y^2 + c_2 z^2; \end{aligned} \tag{A2-13}$$

where a$_1$, a$_2$, b$_1$, b$_2$, c$_1$,c$_2$ are the microscope correction factors. In Figure 2.8, we show the numerical result for the microscope correction factors as function of physical depth with the following parameters: σ_0 =55.5°, λ=590 nm, n_0 = 1.5443 and n_e = 1.7411.

(b) The nematic director makes an angle of 45°with x ($\gamma = \pi/4$):

In this case, $\hat{c} = \frac{\sqrt{2}}{2}\hat{x} + \frac{\sqrt{2}}{2}\hat{y}$ and $\hat{k} = \sin\sigma\cos\phi\hat{x} + \sin\sigma\sin\phi\hat{y} + \cos\sigma\hat{z}$. $\hat{e}$ and $\hat{o}$ can be obtained according to:

$$\begin{aligned} \hat{e} &= \frac{\cos^2\sigma + \sin^2\sigma(\cos\phi\sin\phi - \sin^2\phi)}{\sqrt{1+\cos^2\sigma - \sin^2\sigma\cos\phi\sin\phi}}\hat{x} - \frac{\cos^2\sigma + \sin^2\sigma(\cos^2\phi - \cos\phi\sin\phi)}{\sqrt{1+\cos^2\sigma - \sin^2\sigma\cos\phi\sin\phi}}\hat{y} - \frac{\sin\sigma\cos\sigma(\cos\phi + \sin\phi)}{\sqrt{1+\cos^2\sigma - \sin^2\sigma\cos\phi\sin\phi}}\hat{z}; \\ \hat{o} &= -\frac{\cos\sigma}{\sqrt{1+\cos^2\sigma - \sin^2\sigma\cos\phi\sin\phi}}\hat{x} + \frac{\cos\sigma}{\sqrt{1+\cos^2\sigma - \sin^2\sigma\cos\phi\sin\phi}}\hat{y} + \frac{\sin\sigma(\cos\phi - \sin\phi)}{\sqrt{1+\cos^2\sigma - \sin^2\sigma\cos\phi\sin\phi}}\hat{z} \end{aligned} \tag{A2-14}$$

Similarly, we can obtain the emission amplitude parallel to $\hat{x}', \hat{y}'$ through the liquid crystal in objective space:

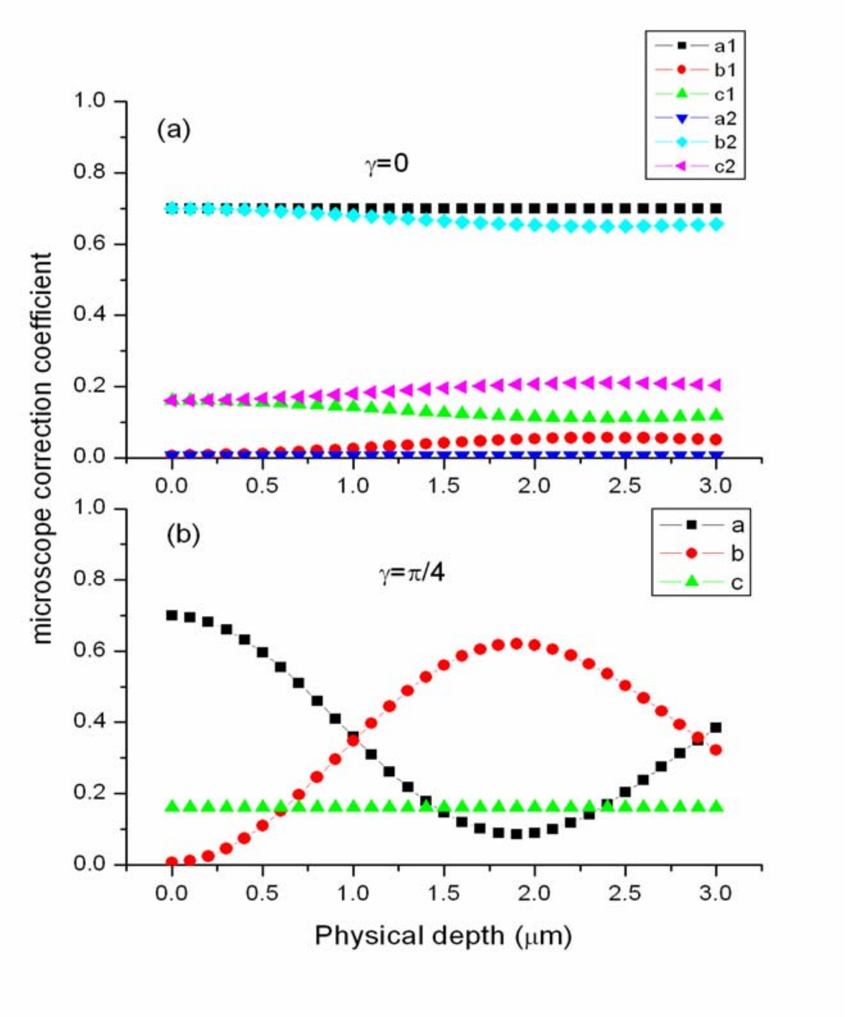

Figure 2.8. Microscope correction coefficient *v.s.* physical depth of polymer in liquid crystal at (a) $\gamma=0$ (referring to A2-13) and (b) $\gamma=\pi/4$ (referring to A2-18). (a) a_1 (square), a_2 (down triangle) are invariant. b_1 (circle) and b_2 (diamond), c_1 (up triangle) and c_2 (tilted triangle), vary slightly in opposite phase with physical depth. (b) a (square), b (circle) vary significantly in opposite phase, and c (up triangle) is invariant. The microscope correction coefficients are calculated by $\sigma_0=55.5°$, $\lambda=590$nm, $n_0=1.5443$ and $n_e=1.7411$.

$$\begin{pmatrix} x'' \\ y'' \end{pmatrix} = \frac{1}{1+\cos^2\sigma - \sin^2\sigma\cos\phi\sin\phi}\begin{pmatrix} A & B \\ -B & A \end{pmatrix}\begin{pmatrix} e^{i\delta} & 0 \\ 0 & 1 \end{pmatrix}$$

$$\begin{pmatrix} (\cos^2\sigma + \sin^2\sigma(\cos\phi\sin\phi - \sin^2\phi))x - (\cos^2\sigma + \sin^2\sigma(\cos^2\phi - \cos\phi\sin\phi))y - \sin\sigma\cos\sigma(\cos\phi + \sin\phi)z \\ -\cos\sigma x + \cos\sigma y + \sin\sigma(\cos\phi - \sin\phi)z \end{pmatrix} \tag{A2-15}$$

where $A = \cos\sigma\cos^2\phi + \cos\sigma\cos\phi\sin\phi + \sin^2\phi - \cos\phi\sin\phi$ and

$B = \cos\sigma\sin^2\phi + \cos\sigma\cos\phi\sin\phi + \cos^2\phi - \cos\phi\sin\phi$

This gives:

$$\begin{aligned} x' = {} & (\frac{(1-e^{i\delta})(\cos^2\sigma\cos\phi\sin\phi + \cos\sigma\cos^2\phi + \cos^2\sigma\sin^2\phi - \cos\sigma\cos\phi\sin\phi)}{1+\cos^2\sigma - 2\sin^2\sigma\cos\phi\sin\phi} + (\cos\sigma\cos^2\phi + \sin^2\phi)e^{i\delta})x \\ & + (\frac{(e^{i\delta}-1)(\cos^2\sigma\cos\phi\sin\phi + \cos\sigma\cos^2\phi + \cos^2\sigma\sin^2\phi - \cos\sigma\cos\phi\sin\phi)}{1+\cos^2\sigma - 2\sin^2\sigma\cos\phi\sin\phi} + (\cos\sigma\cos\phi\sin\phi - \cos\phi\sin\phi)e^{i\delta})y \\ & + (\frac{(e^{i\delta}-1)(\cos\sigma\sin\sigma\sin^3\phi + 2\sin\sigma\cos^2\phi\sin\phi - \cos\sigma\sin\sigma\cos^2\phi\sin\phi - \sin\sigma\cos\phi)}{1+\cos^2\sigma - 2\sin^2\sigma\cos\phi\sin\phi} - \sin\sigma\cos\phi e^{i\delta})z \end{aligned} \tag{A2-16}$$

$$\begin{aligned} y' = {} & (\frac{(e^{i\delta}-1)(\cos^2\sigma\cos\phi\sin\phi + \cos\sigma\sin^2\phi + \cos^2\sigma\cos^2\phi - \cos\sigma\cos\phi\sin\phi)}{1+\cos^2\sigma - 2\sin^2\sigma\cos\phi\sin\phi} + (\cos\sigma\cos\phi\sin\phi - \cos\phi\sin\phi)e^{i\delta})x \\ & + (\frac{(1-e^{i\delta})(\cos^2\sigma\cos\phi\sin\phi + \cos\sigma\sin^2\phi + \cos^2\sigma\cos^2\phi - \cos\sigma\cos\phi\sin\phi)}{1+\cos^2\sigma - 2\sin^2\sigma\cos\phi\sin\phi} + (\cos\sigma\sin^2\phi + \cos^2\phi)e^{i\delta})y \\ & + (\frac{(e^{i\delta}-1)(\cos\sigma\sin\sigma\cos^3\phi + 2\sin\sigma\cos\phi\sin^2\phi - \cos\sigma\sin\sigma\cos\phi\sin^2\phi - \sin\sigma\sin\phi)}{1+\cos^2\sigma - 2\sin^2\sigma\cos\phi\sin\phi} - \sin\sigma\sin\phi e^{i\delta})z \end{aligned} \tag{A2-17}$$

Therefore we can get:

$$I_{\hat{x},\hat{y}} = \int_0^{\sigma_0} d\sin\sigma \int_0^{2\pi} d\phi (x', y')^2$$

Thus,

$$\begin{aligned} I_{\hat{x}} &= ax^2 + by^2 + cz^2; \\ I_{\hat{y}} &= bx^2 + ay^2 + cz^2; \end{aligned} \tag{A2-18}$$

Figure 2.8b shows the microscope correction factors as a function of physical depth with the same parameter as for $\gamma = 0$.

2.4.3 APPENDIX C: SIMULATION OF EMISSION POLARIZATION OF CONJUGATED POLYMER AS FUNCTION OF DEPTH INSIDE A LC MATRIX

In this appendix, we simulate the peak of the polarization histogram for $\gamma = 0$ and the width of the polarization histogram for $\gamma = \pi/4$ as a function of physical depth of the focus in the liquid crystal. This simulation is performed for M98 with and without the effect of shotnoise. Figures 2.9a and 2.9b show the simulation and experimental results for $\gamma = 0$ and $\gamma = \pi/4$, respectively. For the peak of the polarization histogram at $\gamma = 0$, the simulation result indicates that the value does not vary with physical depth within the experimental error. The peak value is the same with and without shotnoise because shotnoise broadens only the width of polarization histogram. In the case of $\gamma = \pi/4$, the width varies much more without including the effect of shotnoise compared to the simulations with shotnoise. This is clearly shows that the broadening due to shotnoise reduces the variation of width caused by the birefringence of the liquid crystal. As shown in Figure 2.9b, the simulation results including shotnoise are within the experimental error. Notice that the experimental width at a physical depth of 0 μm is almost identical to that at 0.5 μm, which is our standard experimental condition. Comparing the experimental to simulation results suggests that we can fit the polarization histograms assuming a physical depth of 0 μm, and the birefringence of the liquid crystal does not alter our conclusions.

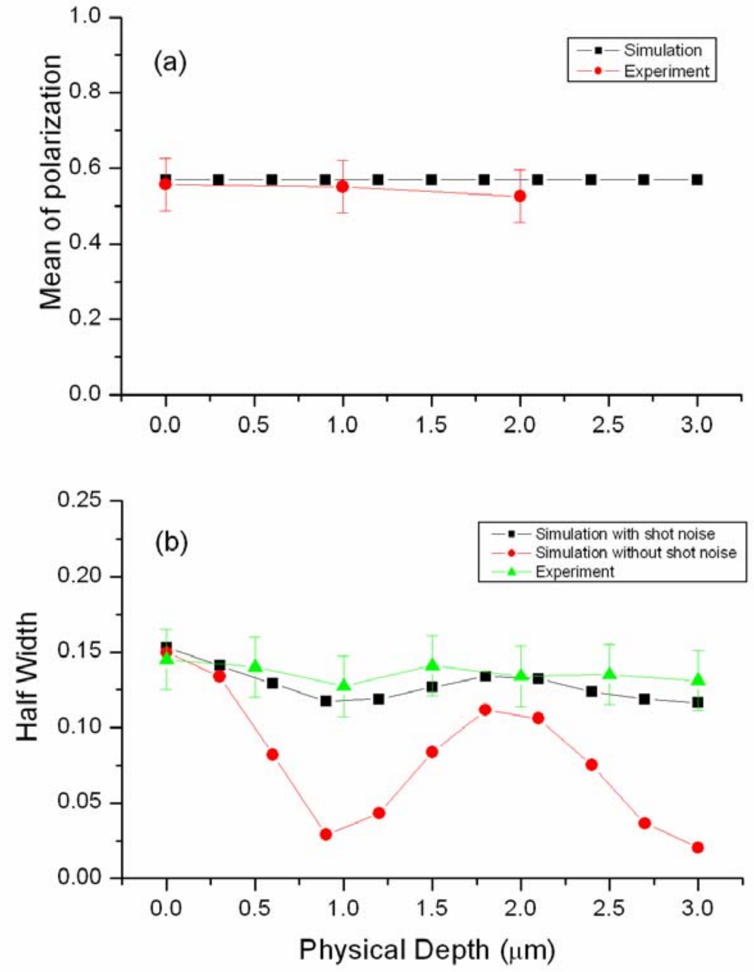

Figure 2.9. (a) The mean of the polarization distribution vs. physical depth at γ = 0. The experimental result (circles) is similar to the values obtained from simulation (squares). The simulation results show that the mean polarization is independent of the physical depth at which the dipole emitters are located. (b) Half width of the polarization distribution vs. physical depth at γ = π/4. The experimental result (triangles) is similar to the simulation (squares) when shot noise is included. The simulation without shot noise (circles) predicts a larger dependence of the polarization distribution on the physical depth.

Chapter 3: Nematic Solvation of Segmented Polymer Chains

3.1 INTRODUCTION

Onsager[80] first predicted that in a binary "solution" of long and short rods, the long rods experience an enhanced alignment in the nematic environment of the shorter rods.[81] The first compelling experimental evidence for this type of "anisotropic solvation" has only been reported recently for single polymer molecules.[82,83] Large single semiflexible biopolymers in the nematic phase of rodlike *fd* virus were visualized directly by fluorescence imaging[82] and found to undergo a coil-rod transition at the isotropic-nematic phase transition. Independently, polarization sensitive single molecule spectroscopy (SMS) revealed that conjugated polymer (MEH-PPV) chains dissolved in a single liquid crystal of 5CB are nearly perfectly aligned with the nematic director of the liquid crystal (LC).[83] Here using SMS and beads-on-a-chain simulations, we explore the effect of polymer chain segmentation on the alignment and elongation in a nematic environment for a series of conjugated MEH-PPV polymers for which synthetic introduction of single bonds at various double bond locations create a controllable number of rigid polymer segments separated by single bonds. For chains with only a few segments, anisotropic solvation due to the nematic solvent is observed to highly elongate the chains. As the number of polymer segments is increased the chains become less elongated due to an interplay among conformational entropy, anisotropic solvation, and the bending energy of the polymer. In addition, highly segmented chains in nematic solvents are observed by simulation to posses low energy "hairpin turn" defects that can dramatically decrease the extension ratio without a significant energy penalty from solvation or bending

3.2 RESULTS AND DISCUSSION

Polymer chains of three different MEH-PPV compounds, denoted by MX (i.e. M98, M70, and M45, where X is 100 minus the percentage of tetrahedral defects[84]) were investigated. The chains were isolated at high dilution in a single domain nematic 5CB liquid crystal[83,85] (2.5 cm x 2.5 cm x 50 μm) at 22 C. Data were acquired in a home-built confocal microscope in either **emission-mode** (i.e. two orthogonally polarized detector systems each with an APD detector), or **excitation mode** (i.e. one unpolarized detection channel but two orthogonally polarized excitation beams that were synchronously chopped at 10 kHz).

Individual polymer molecules diffusing through the excitation volume gave rise to fluorescence bursts. For **emission-mode** the polarization ratio was determined for each burst as $P = (I_{y,em} - I_{x,em}) / (I_{y,em} + I_{x,em})$, where $I_{x,em}$ and $I_{y,em}$ are the x and y polarized florescence intensities. For **excitation-mode** $P = (I_{y,exc} - I_{x,exc}) / (I_{y,exc} + I_{x,exc})$, where $I_{x,exc}$ and $I_{y,exc.}$ are the fluorescence intensities of the single APD detector, with x and y polarized excitation. Histograms of P were generated from several thousand bursts and are shown in Figure 3.1 for M98, M70, and M45. Each panel shows a histogram for three sample orientations where the LC director is either aligned along the x-axis giving rise to negative P values, aligned along the y-axis giving rise to positive P values, or aligned at an angle of 45° to the x-axis leading to P values centered around zero.

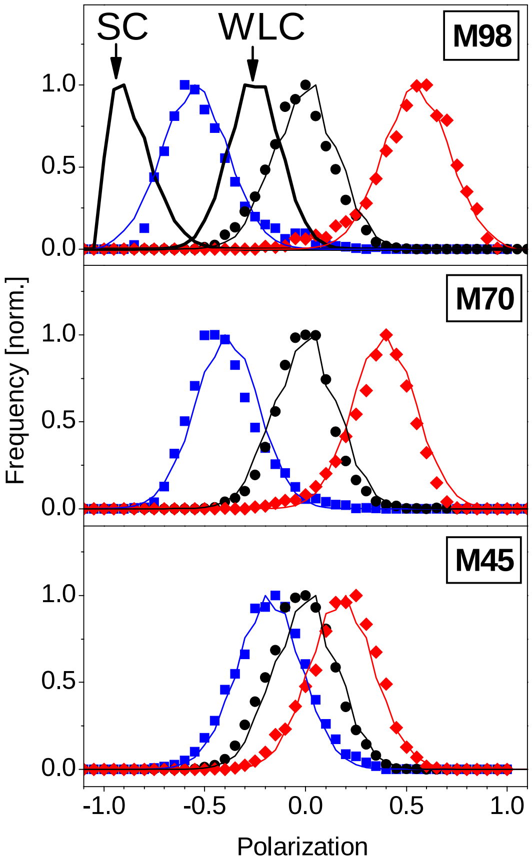

Figure 3.1 Experimental polarization histograms (symbols) for M98 (top), M70 (middle), and M45 (bottom) and fits (lines). Distributions collected in excitation mode were indistinguishable from the emission mode for M98 (not shown). The two limiting cases of a straight-chain (SC) and a worm-like chain (WLC) with the appropriate 2% of defects are included as solid lines (top). The excitation wavelengths were 457 nm for M45 and 488 nm for M98 and M70. The average excitation power was 100-200 nW.

Single conjugated polymer chains are well described as a multi-chromophoric system in which a chromophore consists of 10–15 repeat units.[86] The P values are a measure of the "polarization" of the molecular transition dipole for each chain,

$$P_{chain} = \left(\sum_i \mu_{ix'}^2 - \frac{1}{2} \sum_i (\mu_{iz'}^2 + \mu_{iy'}^2) \right) \Big/ \left(\sum_i \mu_{ix'}^2 + \frac{1}{2} \sum_i (\mu_{iz'}^2 + \mu_{iy'}^2) \right) \tag{3-1}$$

where $\vec{\mu}_i$ is the transition dipole of the i$^{\text{th}}$ segment and cylindrical molecular symmetry is assumed. Model calculations (described below) demonstrate that, due to the relatively low free energy cost of aligning the chains along the nematic director, the chains are well aligned with an orientational order parameter S_O which approaches unity and far exceeds the 0.48 value for 5CB[87] (i.e. $S_O = < \frac{3}{2}\cos^2\alpha - \frac{1}{2} >$ where α is the tilt angle between the major axis of the chain and the director). In analogy to the molecular orientational order parameter, S_O, a conformational order parameter can be defined as, $S_C = < \frac{3}{2}\cos^2\beta - \frac{1}{2} >$ where β is the angle between each segment and the polymer principle internal axis (x'), i.e. the direction of maximum orientation.

The alignment of a long rigid rod present at low mole fraction in the nematic phase of short rods can be understood through an extension of Onsager's description of the orientation-dependent excluded volume of rod-shaped molecules.[81] However, the alignment of a segmented polymer is a considerably more complex problem. For example, the free energy contribution from each segment along the chain can be summed, but the distribution functions describing their orientations are entangled because the segments are linked. By investigating a series of polymers with varying sizes of rigid segments we are able to obtain insights into the synergistic orientation of the segments. In order to elucidate a meaningful structural model that reflects our observations we need to define two kinds of order parameter: one for the polymer, which is essentially an ensemble of segments, S_0, and one for the orientation distribution of segments within the polymer chain, S_c.

It is interesting to compare the experimental M98 results (only 8 defects per chain on average) with theoretical predictions for two limiting cases, i.e. a fully elongated, rigid straight-chain (SC) and a worm-like chain (WLC) with the appropriate 2% of defects, as shown in Figure 3.1. The theoretical predictions include effects due to photon shot-noise and the high numerical aperture of the objective.[88] The experimental M98 values fall intermediate between the fully elongated (P_{chain} = 1) and the WLC isotropic chain limits. The decrease in P values with increasing number of segments along the polymer chains demonstrate that segmentation resists the elongation process. The excitation (not shown) and emission polarization distributions for M98 are indistinguishable, which is consistent with the expectation that the observed P values are not distorted by energy transfer effects.[89] It should be emphasized that this analysis demonstrates that the observed P values are significantly smaller than the actual P_{chain} values due to the high numerical aperture of the objective that collects and excites with z-component light, lowering the detected polarization in the emission-mode and excitation-mode experiments, respectively.

Further insight into the anisotropic solvation of segmented polymer chains was obtained by Monte Carlo (MC) simulations by adopting our previous model[7,8] for segmented conjugated polymers, i.e. a chain of 100 hard beads connected by bonds with a chain bending energy, $E_{bend} \sim 10\ k_B T rad^{-2} \cdot \psi^2$, where ψ is the angle difference from the equilibrium bond angle (180° for normal bonds and 109.5° for the tetrahedral defects that join each segment). The model was adapted by introducing a mean-field anisotropic solvation potential[90] per repeat unit, V_{RU}, of the polymer chain,

$$V_{RU}(\chi) = -\tfrac{3}{2} v_{RU} \cos^2 \chi < \tfrac{3}{2}\cos^2 \gamma - \tfrac{1}{2} > \quad (3\text{-}2)$$

where v is the solute-solvent intermolecular interaction strength, χ is the angle of the each repeat unit (and associated segment) relative to the nematic director, and γ is the angle of each LC solvent molecule relative to the director. Since the polymer chains are highly dilute we use the order parameter of 5CB for the required value in Eq. (3-2), i.e. $< \tfrac{3}{2}\cos^2 \gamma - \tfrac{1}{2} >\ = 0.48$.[87] Furthermore, since a MEH-PPV repeat unit is similar in chemical properties to 5CB but roughly 1/3 smaller in size, we use ~1/3 of the v value for 5CB, i.e. $v_{5CB} = 4.6\ k_B T$ for 5CB and $v_{RU} = 1.4\ k_B T$ for each bead-length on the chain. In addition, the intra-chain interaction potential was assumed to be repulsive, consistent with SMS polarization selection experiments that indicate that MEH-PPV adopts and an "un-collapsed" conformation in 5CB.[89] Figure 3.2 illustrates simulated normalized absorption cross-sections (a,d) along the three principal axes of the conformation and orientation angle α (b,e) versus MC simulation step for a polymer with 15 and 50 defects. Initially the LC anisotropic solvation energy is set to zero, and is turned on after 1000 steps. Upon its inclusion, the shape of the molecule becomes more anisotropic (elongated), observed as an increase in the absorption cross-section of the major axis, and a corresponding decrease in that of the

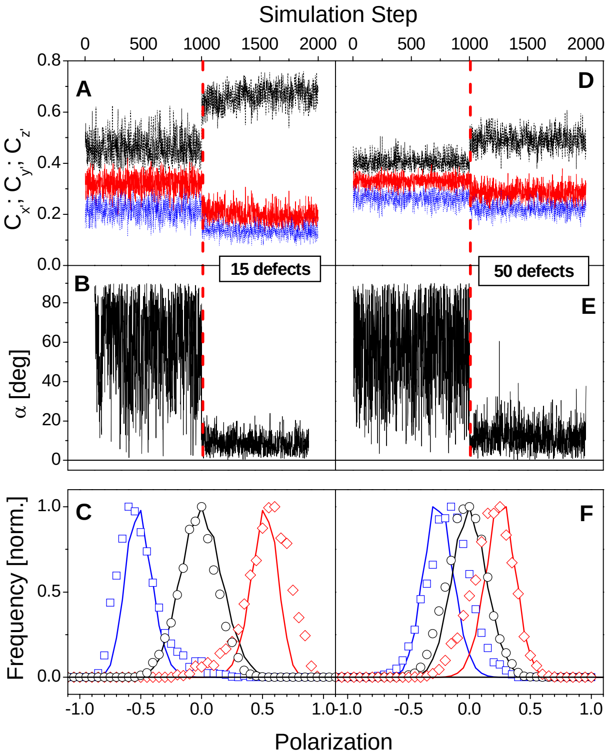

Figure 3.2 Normalized absorption cross sections along the three principal axes of the conformation (a,d) and orientation angle α (b,e) versus MC simulation step for a polymer with 15 (left) and 50 defects (right). (c,e) Polarization histograms calculated from the MC conformations (lines) compared to the measured polarization distribution (symbols) for M98 (left) and M45 (right).

two minor axes. The mean field potential also forces the major axis of the molecule to align with the LC nematic director. This is further illustrated in Figure 3.3, which shows two typical conformations of a 100-segment homopolymer with 15 defects without (a) and with (b) the LC potential. The nematic director is parallel to the x-axis. Correspondingly, (c) and (d) show typical conformations for a chain with 50 defects.

Figure 3.2(c) and (f) show a comparison of the simulated and experimentally observed polarization distributions demonstrating good qualitative agreement. The numbers of defects per chain were adjusted arbitrarily to get good agreement between the simulated and observed P data. It is not surprising that the number of defects in the best-fit simulation differs significantly from the actual number of defects, considering the simplicity of the model and that it was necessary due to limited computational resources to simulate chains with a much smaller number of repeat units compared to the experimental chains. For the theoretical framework applied herein, S_C and P_{chain} are simply related by $P_{chain} = 3S_C/(2+S_C)$. Simulated conformational order parameters, and orientational order parameters are summarized in Figure 3.4 (bottom) verifying the expected decrease in both types of order with increasing number of segments. Most striking are the large values for both order parameters even for the polymers with a large number of segments. Figure 3.4 (bottom) also portrays the modified extension ratio R_{ER} for the chains, which we define as the equilibrium end-to-end distance $<r^2>^{1/2}$ in the LC environment normalized by the end-to-end distance of a purely elongated but non-bent

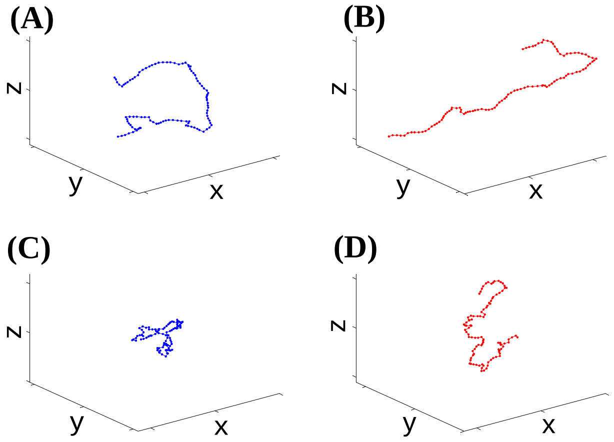

Figure 3.3 (A,B) Typical conformation of a 100-segment homopolymer with 15 defects generated by MC simulations without (top left) and with (top right) a liquid crystal environment. (C,D) Corresponding conformations for a polymer with 50 defects.

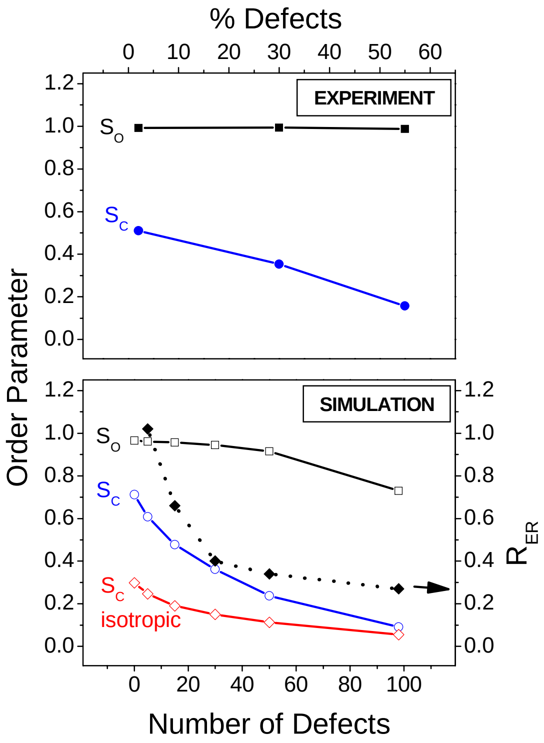

Figure 3.4 External (S_O) and internal (S_c) order parameters as a function of defect concentration for the three polymer samples (top). The bottom panel shows the order parameters for the simulated polymers as a function of defects including the modified extension ratio and the internal order parameter for chains simulated without the LC potential. The lines only serve as a visual guide.

chain. The simulated polymer chain with 5 defects in fact approaches the fully unbent, fully elongated limit (R_{ER} = 1) indicating the ability of the nematic environment to actually stretch the chain with a small number of defects (assumed to be equally distributed along the chain). It should be noted however that for a highly segmented polymer, such as that shown in Figure 3.3(d), the nematic environment can align segments of the polymer without elongating the polymer by forming hairpin turns in the chains, which when induced by single bond defects have little energy penalty over more elongated defect geometries, e.g. a chain zig-zag. A similar interplay between the anisotropic solvation and the intrinsic flexibility of main-chain nematic polymers with flexible spacers between mesogenic groups has previously been inferred from small angle neutron scattering[91] and viscosity[92,93] measurements.

The bottom panel in Figure 3.4 shows that the simulated orientational order parameters are much greater than the conformational order parameters, demonstrating that the chains are well aligned along the nematic axis and the predicted P values primarily reflect conformational order. The decreases in S_O with decreasing S_C can be traced in this model to the direct dependence of the solvation energy per molecule on S_C as follows,

$$V_{chain}(\alpha) = -\tfrac{3}{2} N_{RU} v_{RU} S_c \cos^2\alpha < \tfrac{3}{2}\cos^2\gamma - \tfrac{1}{2} > \qquad (3\text{-}3)$$

where N_{RU} is the number of repeat units per chain. The solid lines in Figure 1 show a best fit (not a simulation) of the model implied by Eqs. (3-1) and (3-3) to the experimental data giving excellent agreement. The top panel of Figure 3.4 summarizes the order parameters obtained from the fit. This comparison of model and experiment also indicates that the orientational order is much greater than the conformational order and that increasing segmentation decreases conformational order.

3.3 CONCLUSION

In conclusion, we have used polarization SMS and coordinated simulations to explore how polymer segmentation effects the elongation and alignment of polymer chains in a nematic environment.

Chapter 4: Orthogonal Orientations for Solvation of Polymer Molecules in Smectic Solvents

4.1 INTRODUCTION

The nature of the solvent plays an important role in the conformational properties and structure of stiff polymers in solution. Depending on the solvent quality and intra-molecular interactions, the polymer molecules can be extended (rod-like), collapsed, toroidal or even in a nano-nematic state where the segments of the locally rod-like polymer pack together like flower stems in a bouquet.[7,94,95] A particularly interesting case is when the solvent itself possesses order, as is the case of a nematic liquid crystalline solvent[52,55]. In this case long rod-like polymer molecules align along the nematic director to a much greater degree than the solvent molecules themselves because longer rods experience the local nematic field over much larger distances than the solvent nematogens. This striking effect, previously inferred from small angle neutron scattering[96] and viscosity measurements[97], was recently measured directly, using single molecule spectroscopy, for solutions of conjugated polymers[52,55] and colloidal virus particles[98].

In this work we investigate, using single molecule spectroscopy, the solvation of a polymer molecule in a *smectic* liquid crystal (LC). In an ideal smectic A phase, the solvent molecules are aligned preferentially along a particular direction (called the director) as in a nematic phase, but in addition there are layers. Within each layer the arrangement of molecules is liquid-like, but the layers stack above each other in a one-dimensional crystalline array[22]. This is clearly an idealization, however, x-ray scattering experiments[99-101] have demonstrated quite convincingly that the variation of the average density along the director is *sinusoidal* in thermotropic smectics, in agreement with theory[102]. Very little is known regarding the effect of smectic solvation on the properties of single polymer molecules. We study this phenomenon using single molecule polarization spectroscopy of the rod-like polymer MEH-PPV dissolved in the smectic phase of a solvent composed of 8CB molecules.

4.2 RESULTS AND DISCUSSION

We discover that there are two distinct, orthogonal orientations for the polymer solute (Figure 4.1, top). In the majority of cases, the polymer molecules are aligned parallel to the director as is seen when the solvent is in the nematic phase. Surprisingly about 10% of the polymer molecules are aligned *perpendicular* to the director. Such an orientation seems possible in an ideal smectic material where the polymers might fit into the “empty spaces” between layers. But how is this possible in a material with only a sinusoidal density variation and no real “gaps”? We suggest that the polymer molecules insert into the low-density inter-layer region by *creating space* for themselves. The single molecule measurements therefore reveal interesting information regarding the local structure that is not accessible in ensemble x-ray measurements. The experiments

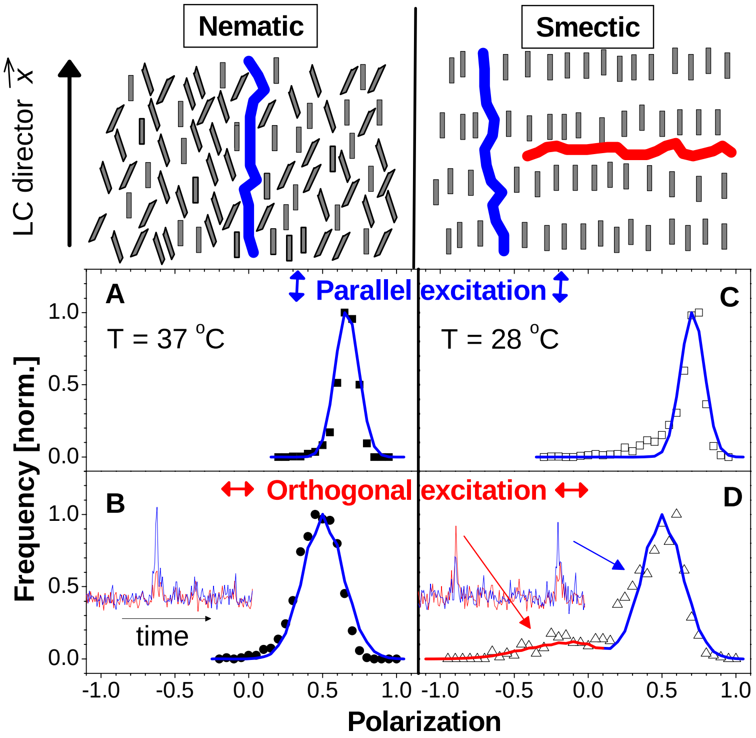

Figure 4.1 Orthogonal orientations for solvation of MEH-PPV in a smectic LC. Top: Schematic picture of the nematic (left) and ideal smectic (right) LC phase. In the nematic phase, the solvent molecules (indicated by cylinders) have an orientational order with an alignment of the main molecular axis parallel to the LC director. In the ideal smectic phase, the solvent molecules posses positional order along the director forming two-dimensional layers. Solvation of larger polymers (not scaled) is indicated by the blue and red chains. In the ideal smectic phase, the polymers can create gaps between layers. Bottom: *P* histograms measured with excitation polarized parallel (A,C) and orthogonal (B,D) to the director. The insets show a typical fluorescence burst from a single polymer molecule diffusing through the excitation volume. Positive *P* is consistent with parallel alignment to the director (blue chain). For orthogonal excitation in the smectic phase (D), the fluorescence transient reveals the presence of molecules with an opposite *P*. These molecules are orientated perpendicular to the director (red chain). The corresponding *P* histogram shows that a small fraction (~ 10%) of polymer molecules is aligned perpendicular with a larger degree of disorder. The solid lines are fits to the histograms.

suggest the intriguing possibility of using long chains as a molecular scaffold for creating a new class of tunable nano-structured materials.

Isolated MEH-PPV polymer chains, dissolved in a single domain LC that is mounted inside a temperature-controlled cell, are studied by confocal microscopy[55]. The microscope is equipped with two orthogonally polarized detector systems allowing us to measure the polarization ratio P for each single polymer molecule diffusing through the excitation volume according to $P = (I_{\parallel} - I_{\perp})/(I_{\parallel} + I_{\perp})$. $I_{\parallel}$ and $I_{\perp}$ are the fluorescence intensities polarized parallel and perpendicular to the LC director. The sign of P expresses the relative orientation of the main polymer axis: Positive values indicate parallel alignment of the polymer chain and negative values indicate perpendicular alignment.

Figure 4.1 shows P histograms for MEH-PPV in the nematic (left) and smectic (right) phase of 8CB as well as two typical intensity trajectories (insets). For the nematic phase, all polymer molecules are aligned parallel to the director (left scheme on top of Figure 4.1). For the smectic LC phase, two orthogonal polymer orientations are observed, indicated by the reversal of intensity ratios for different fluorescence bursts and the appearance of an additional broad distribution in the P histogram peaked at negative P values (Figure 4.1D). Similar diffusion constants for MEH-PPV in both orientations as obtained from autocorrelation analysis (not shown) confirm the concept of a second solvation site.

We hypothesize that the perpendicular aligned polymer molecules occupy gaps in between the solvent layers formed in the smectic phase (right scheme on top of Figure 4.1). The perpendicular solvation site is emphasized in the P histogram by using orthogonal excitation, which selectively excites the chromophores orientated perpendicular to the director. For orthogonal excitation (Figure 4.1B and 4.1D), the peak of the positive *P* is shifted towards smaller values due to the selective excitation of chromophores tilted away from the director. This is consistent with independent observations that energy transfer is insignificant for extended MEH-PPV conformations solvated in a LC[55].

The perpendicular alignment inferred from the negative *P* values is assigned to a local minimum in the smectic solvation potential. The absence of a change of the polarization ratio during a fluorescence burst implies a large energy barrier for the inter-conversion between the solvation sites. Using parallel excitation, the histogram for the smectic phase also exhibits a tail towards smaller *P* (Figure 4.1C). This tail can be attributed to polymer molecules aligned with a main part of their chain parallel to the director and a shorter segment bent perpendicular into inter-layer channels. Such bends in the polymer chain have been observed in beads-on-a-chain simulations where MEH-PPV is represented by stiff segments interrupted by tetrahedral defects[7]. With roughly 8 defects per chain for our MEH-PPV sample, these bends should be energetically favorable over more severe hairpin-like turns found for nematic solvation of MEH-PPV[55]. Such "L-shaped" conformations can also contribute to the negative *P* distribution when using orthogonal excitation.

Computer simulations of small bent molecules (azobenzene derivatives) dissolved in smectics show that these molecules segregate to the inter-layer region[103,104]; a segregation that is accompanied by an increase in the inter-layer spacing[101,103,105,106]. It is possible that this effect plays a role in the perpendicular solvation of the MEH-PPV polymers as well. A big difference between the solvation of polymers and small molecules, of course, is that the polymers interact with the solvent on length-scales that are two orders of magnitude larger. Local effects are therefore expected to be less important for polymers than small molecule solutes.

The ordering of the polymer along the director increases with decreasing temperature without a discontinuous change at the smectic-nematic phase transition (see Figures. 4.2 and 4.3). The absence of a pronounced phase transition for P is consistent with a second[107] or weak first[108] order phase transition reported for the solvent order parameter and is further obscured by the stiffness and length of the individual polymer segments (~ 50 monomers). Possible local fluctuations of the layers could also be responsible for the observed insensitivity[22]. The observed P histograms and fractional population of the orthogonal solvation sites is reproducible for repeated temperature cycling between different LC phases, including the isotropic phase (not shown), indicating that the observed distributions reflect the equilibrium state of the systems (see Figure 4.2).

We have shown previously[55] that the measured P values for single conjugated polymer molecules dissolved in a nematic LC can be quantitatively modeled to determine the orientational distribution of polymer segments with respect to the director of a LC, allowing for information on how anisotropic solvation impacts the orientation and conformation of polymer chain solutes. The large positive P values in all the histograms shown in Figure 4.1 indicate a high degree of order of the MEH-PPV molecules parallel to the director that far exceeds the order parameter of the 8CB solvent (i.e.

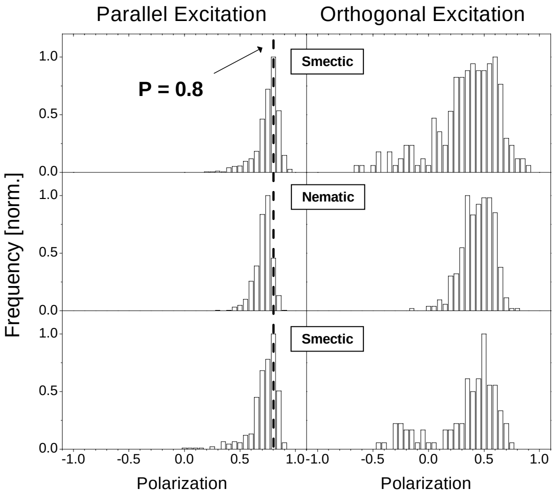

Figure 4.2 *P* histograms using parallel (left) and orthogonal excitation (right). The temperature is varied from 28 to 37 and back to 28 °C (top to bottom) cycling between the smectic and nematic LC phases. The *P* histograms on the right show a second distribution with negative *P* values indicating polymer molecules aligned perpendicular to the director in the smectic phase (top and bottom), which is absent in the nematic phase (middle) and for a sample containing only 8CB (not shown). For parallel excitation (left, 488 nm, 1 kW/cm^2), the maximum of the *P* histogram shifts to smaller values in the nematic compared to the smectic phase (see line for *P* = 0.8). This is due the increased stretching of the polymer chain with increasing order of the LC solvent molecules (see Figure 3).

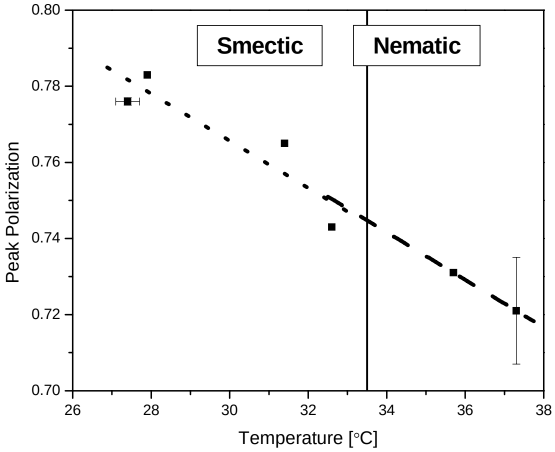

Figure 4.3 Peak *P* as a function of temperature. *P* increases roughly linearly with temperature in the studied temperature range from 27 to 37 °C across the smectic-nematic phase transition. The lines are independent linear fits to *P* in the smectic and nematic LC phases demonstrating the lack of a strongly discontinuous phase transition for *P*. The decrease of *P* with increasing temperature can be explained by a decrease in conformational order of the polymer chain due to a lower solvation energy counteracting the intrinsic bending energy and conformational entropy of the chain. (The shown error bars are representative for all data points.)

$S_O = < \frac{3}{2}\cos^2\alpha - \frac{1}{2} > \sim 1$ where α is the tilt angle between the major axis of the chain and the LC director). An analysis of the single molecule *P* values herein show that for the parallel site in the smectic solvent, the MEH-PPV chain segments are aligned with the director to a much greater degree than in the nematic phase with molecular polarization values of $P_{chain} \sim 0.75$. P_{chain} is defined as

$$P_{chain} = \left(\sum_i \mu_{ix'}^2 - \frac{1}{2}\sum_i (\mu_{iz'}^2 + \mu_{iy'}^2) \right) \Big/ \left(\sum_i \mu_{ix'}^2 + \frac{1}{2}\sum_i (\mu_{iz'}^2 + \mu_{iy'}^2) \right),$$

where $\vec{\mu}_i$ is the transition dipole of the ith polymer segment, and is related to the internal conformational order parameter $S_C = < P_2(\cos\beta) > = < \frac{3}{2}\cos^2\beta - \frac{1}{2} >$ according to $P_{chain} = 3S_C/(2+S_C)$. β is the angle between each segment and the polymer principle axis (x'-axis). These model calculations also allow for experimentally determined orientational probability distribution function *f(β)* for the segments of the polymer molecules in the parallel and perpendicular solvation sites which are shown in Figure 4.4A and 4.4B together with two representative polymer conformations (C,D)[7,55]. Using a mean field potential, *f(β)* is calculated from the fitted value of P_{chain} with the self-consistent definition of the order parameter $< P_2(\cos\beta) > = \int d\beta \sin\beta\, f(\beta)\, P_2(\cos\beta)$. These results emphasize that there are orthogonal solvation sites for polymer chains in a single smectic LC. The average molecular polarization P_{chain} of the perpendicularly orientated polymer chains is decreased from 0.75 to ≤ 0.5. The broad distribution and smaller P_{chain} of the perpendicularly oriented polymers (Figure 4.4B) reflect a greater degree of disorder. The lower P_{chain} for the perpendicular solvation site may be due to various factors, including: a disordered polymer conformation, a broad orientational

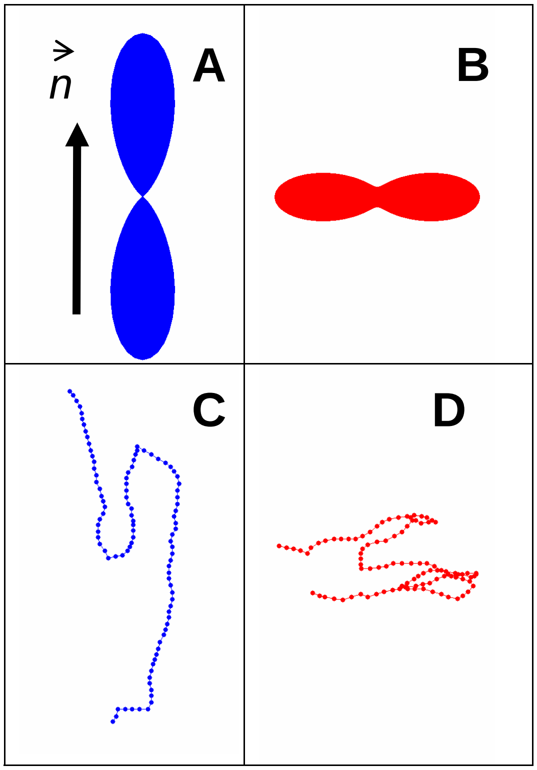

Figure 4.4 Graphical representation of the experimentally determined orientational probability distribution functions for the segments of the polymer molecules in the parallel (A) and perpendicular (B) solvation sites. The average molecular polarizations P_{chain} of the polymer chains are 0.75 and 0.4 for the parallel and perpendicular solvation site, respectively. (C,D) Corresponding conformations of a 100-segment homopolymer generated by beads-on-a-chain simulations. The arrow indicates the direction of the LC director.

distribution, and/or fast molecular rotation in the y-z plane on the time scale of the ~ 50 ms transit time. All three effects are qualitatively consistent with expectations for polymer molecules solvated between layers in a smectic LC.

The experimentally observed perpendicular alignment of MEH-PPV implies the presence of significantly larger inter-layer gaps than in neat 8CB and can be qualitatively understood from a generalization of mean-field theory of the nematic-smectic transition. In the theory of thermotropic LCs the nematic phase becomes stable relative to the isotropic phase (as the temperature is lowered) because the favorable attractive interactions between aligned molecules becomes more significant than the loss of configuration entropy. Similarly, the smectic phase becomes stable relative to the nematic phase because the gain in favorable attractive interactions (when molecules are layered) overcomes the entropic cost of creating these layers. One would expect the entropic cost of creating layers to be reduced if the polymer molecules inhabit the inter-layer region. The presence of polymers therefore stabilizes the layers at a larger separation than in the neat solvent.

4.3 CONCLUSION

In conclusion, we present evidence for two orthogonal solvation sites for the conjugated polymer MEH-PPV dissolved in the smectic LC 8CB. The majority of polymers are aligned parallel to the director with an order parameter approaching unity, while a small fraction (~ 10%) of molecules with a larger degree of disorder fit into inter-layer channels. Our results demonstrate that the polymer chains can be used as sensitive probes of the three-dimensional structure of smectic LCs otherwise inaccessible by other techniques.

Chapter 5: Single Molecule Spectroscopy of Conjugated Polymer Chains in an Electric Field Aligned Liquid Crystal

5.1 INTRODUCTION

Composite materials composed of mixtures of polymeric solutes and liquid crystalline solvents are of interest for a variety of reasons. The anisotropic solvent provides a means of controlling the conformation and orientation of polymer solutes, through solvent-solute interactions. It might therefore be possible to fabricate well organized nano and meso scale polymer structures with important optoelectronics applications.[12,13,109,110] For example, conjugated polymers have been synthesized using a liquid crystal (LC) template in order to enhance the electric properties of the polymer.[12,13] Recent studies have investigated the enhanced alignment of conjugated polymers in a nematic and smectic single LC. In this work we investigate the effect of an external electric field on the polymer alignment in a LC device.

A polymeric solute tends to align with the nematic director of the solvent. Single molecule spectroscopic studies have been used to measure the molecular details of the alignment of polymers dissolved in a LC matrix,[52,55,56,98] and to show that the stiff conjugated polymer MEH-PPV dissolved in the nematic solvent 5CB is elongated and almost perfectly aligned with the nematic director.[52,55,56,60] This solvent-directed alignment of the polymer chains has been explained by a "cooperative solvation" model.[52,55,56] The MEH-PPV molecules, which are about 100 times larger than the 5CB solvent molecules, experience an effective mean solvation potential from a large number of solvent LC molecules, which "cooperatively" force the MEH-PPV to align parallel to the director. Onsager first predicted this phenomenon for a binary solution of long and short rods and found theoretically that in a nematic environment the long rods are highly aligned with the average alignment direction of the short rods (i.e. nematic director).[111] In this chapter, we further explore the alignment of MEH-PPV in a LC solvent with different director orientations, which is achieved through electric field (E-field) induced switching of the orientation of the LC molecules.

The molecules in a nematic phase align in an externally applied E-field above a certain critical threshold voltage V_c.[47]. Above V_c, LC molecules that have a dipole moment parallel to the long molecular axis and hence a positive dielectric anisotropy are attracted by the E-field. The opposite case holds for LC molecules with negative dielectric anisotropy. The transition to this electric field (E-field) induced alignment of the LC molecules is known as the Frederick's transition,[47] and is often studied by electro-optical experiments.[34,112-114] Consider a device consisting of an LC solution sandwiched between two transparent electrodes. In the absence of an E-field the molecules align parallel to the surfaces in a planar alignment. When an E-field above V_c is applied in a direction perpendicular to the surfaces, the molecules are aligned parallel to the E-field, i.e., perpendicular to the LC device. This E-field induced director alignment is referred to as homeotropic alignment. However, the molecules near the device interface remain aligned parallel to the substrate due to strong interactions (i.e. surface anchoring) with a surface alignment layer consisting typically of a polymer coating. The effect of an applied E-field on the local order of LC solvents is of interest in fundamental science and flat-panel display applications. The director orientation at the device interface has been measured by many techniques including optical[24-41] and acoustic[42-45] methods, and has been explained by a elastic continuous theory[46,47].

In this work, we use single molecule spectroscopy to investigate the orientation of MEH-PPV molecules in a nematic LC solvent with and without an applied E-field as a function of distance from the LC substrate interface. We find that the polymer molecules align with the director orientation in the planar and homeotropic case. In addition, for the homeotropic alignment, the experiments show a parallel alignment of polymers near the interface and a perpendicular alignment in the "bulk" region with a continuous change of polymer orientations between the two regions. This suggests that MEH-PPV can be used as a sensitive probe of the local order and dynamics in complex anisotropic media.

5.2 RESULTS AND DISCUSSION

Electro-optical measurements are routinely employed to determine the orientation of LC molecules in a LC device with an applied E-field.[34,112-115] Figure 5.1(A) is a schematic drawing of the setup used for measuring the transmittance through a LC device positioned between two crossed polarizers. The LC director is orientated 45° with respect to both polarizers. Due to the birefringence of the LC molecules, transmittance is observed when LC molecules are aligned parallel to the substrate. In contrast, for LC molecules orientated perpendicular to the substrate, the transmittance decreases to zero because the absence of sample birefringence leaves the polarization of the incident light unchanged. Figure 5.1(B) shows the room temperature electro-optical response of 5CB. In the absence of an E-field, the long axes of the LC molecules are aligned parallel to the surface due to the sample preparation method.

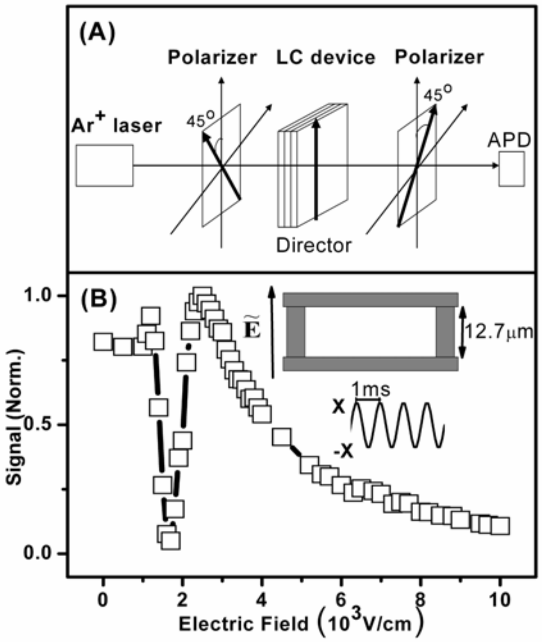

Figure 5.1 (A) Experimental setup for the electro-optical measurements. (B) Electro-optical response of 5CB in a nematic cell at room temperature. Inset: Schematic of the nematic cell and the function of the applied E-field.

Above V_c = 1V, the LC molecules start to align with the E-field because of the positive dielectric anisotropy of 5CB. The change of the LC director orientation in response to an increasing E-field alters the birefringence of the nematic cell and hence the observed transmittance. The transmittance vs. applied field for 5CB, as shown in Figure 5.1(B), is consistent with previously published results.[115] At a voltage of 10V, the extinction of the transmittance indicates that the molecules in the bulk LC solution are aligned parallel to the E-field (perpendicular to the substrate), in the homeotropic alignment. MEH-PPV doped 5CB devices showed similar electro-optical behavior, suggesting that the presence of a low concentration of MEH-PPV does not alter the orientation of the LC during the application of the E-field. All further experiments with applied E-fields were performed at V = 10V ($5.5*10^3$ V/cm RMS voltage).

We have previously shown that MEH-PPV molecules dissolved in 5CB are highly aligned, with an orientation order parameter approaching unity.[52,55,56] This is shown in Figure 5.2(A) and (C), in the form of a schematic drawing and a polarization histogram, respectively. In Figure 5.2(C), the experimental polarization histogram (scatter) is peaked at 0.68 with a standard deviation of 0.10. The single molecule polarization distribution is fit (line) using a conformational order parameter S_c (presenting the averaged conformation of a single polymer chain) of 0.70 and an orientation order parameter S_o (presenting the average orientation of the main polymer axis with respect to the LC director) of 0.99. The theoretical fit is based on an anisotropic mean field solvation model with the assumption that the shape of the polymer chain can be approximated as a cylinder, as described in previous work.[55,56] The effects of shot noise broadening and a high NA objective[70] are also considered in the fitting routine.

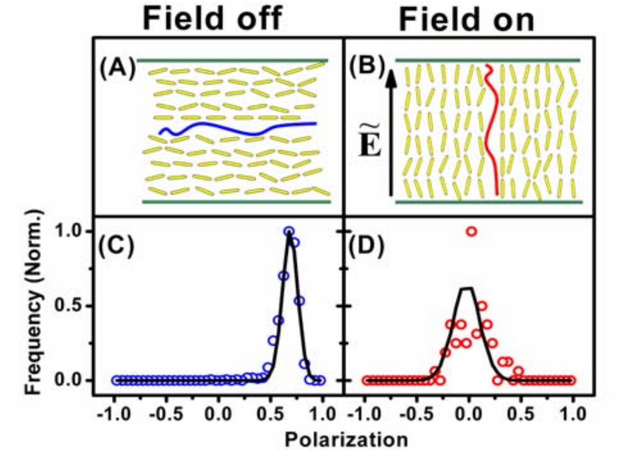

Figure 5.2 Top: Schematic picture showing the orientation of a nematic LC without (A) and with (B) an applied E-field. Solvation of large polymers (not scaled) is indicated by the blue (A) and red (B) chains. Bottom: Experimental polarization histograms (scatter) and corresponding fit (line) obtained without (C) and with (D) applied E-field at 3 μm from the LC-PVA interface.

With an applied E-field, the experimental polarization distribution (scatter) measured at 3 μm inside the cell is now peaked at 0 with a standard deviation of 0.17 (Figure 5.2(D)), indicating a change in the orientation of the MEH-PPV molecules. A polarization histogram peaked at 0 is consistent with three scenarios: (1) a random alignment of fast rotating polymer chains (isotropic alignment), (2) a polymer conformation, with spherical symmetry (3) anisotropic polymer chains that are a perpendicularly aligned with respect to the substrate. An isotropic alignment of the MEH-PPV molecules can be ruled out considering that applying an E-field perpendicular to the substrate causes only a change of the LC director orientation without a change of the LC order parameter[47,116,117].

In order to distinguish between a collapsed spherically symmetric conformation and a perpendicular alignment, the dual channel intensity histograms with and without an applied E-field are compared. The results of this comparison are shown in Figure 3 for a measurement at a depth of 3 μm from the LC-PVA interface without (A) and with (B) an applied E-field. The insets show intensity bursts of a single polymer freely diffusing through the focal volume. Channel 1 and channel 2 each detect one of the two orthogonal polarization components of the fluorescence emitted from within the sample plane. The sample is oriented such that, without an applied E-field, the LC director, and hence the long axes of the MEH-PPV molecules, are oriented parallel to the polarization detected by channel 2. In this case, the burst intensity is much higher in channel 2 compared to channel 1. In Figure 5.3(A), the mean intensities of channel 1 and channel 2 are 40 and 201 (counts/50ms), respectively. In contrast, the burst intensities from the two channels

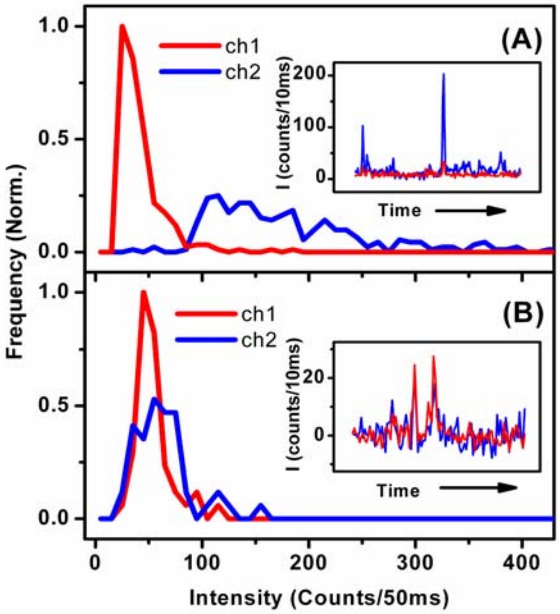

Figure 5.3 Dual-channel fluorescence intensity histograms of MEH-PPV in 5CB without (A) and with (B) an applied E-field at 3 μm from the LC-PVA interface. The insets show intensity bursts from single polymers diffusing through the focal volume.

are almost the same with the E-field applied to the LC cell. This is shown in Figure 5.3(B) where the mean intensities are 54 and 63 counts/50ms for channel 1 and 2, respectively.

A spherically symmetric conformation can be ruled out by comparing the mean intensity of channel 1 and 2 using a simplified model without considering the effect of a high NA objective. The detected intensities of channel 1 and channel 2 depend on the conformation and orientation of the MEH-PPV molecules. In the absence of an external field, the MEH-PPV molecules are modeled as cylinders aligned parallel to the substrate as shown in Figure 5.2(A). The intensities of channel 2 ($I_{ch2,\ planar}$ = 201counts/50ms) and channel 1 ($I_{ch1,planar}$ = 40counts/50ms) measure the fluorescence emitted from the polymer segments in the sample plane parallel and perpendicular to the LC director, respectively. However, because of the collection geometry, fluorescence emitted from polymer chains orientated perpendicular to the substrate and hence polarized along the optical axis (I_z) cannot be detected. For a cylindrical polymer conformation, I_z equals $I_{ch1,\ planar}$ and the total fluorescence intensity emitted from the polymer molecules is then $I_{total} = I_{ch1,\ planar} + I_{ch2,\ planar} + I_z$. Assuming that I_{total} is independent of polymer conformation, the intensities of channel 1 and 2 should be equal to $\frac{1}{3}(I_{ch1,planar} + I_{ch2,planar} + I_z)$ if the polymer conformation becomes spherically symetric in the presence of an E-field. This calculation predicts an intensity of ~ 94 counts/50ms for channel 1 and 2. However, this value is much higher than the measured mean intensities of 54 and 63 counts/50ms for channel 1 and 2, respectively. A spherically symetric polymer conformation can therefore be ruled out. However, if the long axis of the polymer is aligned perpendicular to the substrate without a change of polymer conformation, the intensities of channel 1 and channel 2 should be equal to $I_{ch1,planar}$ (i.e. $I_{ch1,\ homeotropic} = I_{ch2,\ homeotropic}$ = 40 counts/50ms), which is in reasonable agreement with the measured mean intensities of 54 and 63 (counts/50ms). The small shift towards higher values for the observed intensities is due to the high NA objective, which allows for small contributions from I_z to be detected[70].

The measured polarization distribution with an applied E-field can therefore only be explained with a perpendicular alignment of MEH-PPV with respect to the device substrate. The polarization in Figure 5.2D is modeled with such a perpendicular alignment using the same conformational and orientation order parameters as in the case without an applied field. The fact that the same conformational order parameter can be used to model the measured polarization histogram suggests that the polymer chains are equally stretched in the homeotropic alignment compared to the planar alignment. This is in good agreement with the fact that the LC order parameter is unchanged regardless of the director orientation.[47,116,117] This implies that the individual polymer segments always experience the same solvation energy independent of director orientation, consistent with our experimental results. Furthermore, the good fit of the polarization histograms in Figure 2 verifies our model for the anisotropic alignment of polymer chains in a LC host and justifies the assumption made about a cylindrical polymer conformation. The results further support the previously introduced concept of *cooperative anisotropic solvation*. Because a MEH-PPV molecule is about 100 times larger than a 5CB molecule, each polymer experiences a solvation potential equal to that of many (~ 100) solvent molecules added together. The MEH-PPV molecules are therefore perfectly aligned with the nematic director as a result of this large cooperative anisotropic solvation energy, independent of an applied E-field.

However, how do the MEH-PPV molecules align in the vicinity of the device interface? It is well known that the LC molecules near the device interface remain aligned parallel to the substrate due to strong interactions (i.e. surface anchoring) with a surface alignment layer. It is of interest to ascertain if the MEH-PPV molecules can probe this local nematic alignment. Figure 4 shows the polarization histograms for single MEH-PPV chains with field off (left column) and on (right column) for the laser focused at Z = 0 - 3 μm, where Z is the distance between the LC-PVA interface and the position of the laser focal point. In the absence of an applied field, the polarization histograms are almost identical and peaked at 0.68 for Z = 0 - 3 μm. When an AC E-field is applied, the peak of the polarization histogram shifts from 0.6 at Z = 0 μm to 0 at Z > 2 μm. At intermediate distances of Z = 1 and 1.5 μm, the polarization histograms are broad, reflecting a complex LC ordering in the transition region between the surface aligned LC molecules and the electric field orientated bulk of the solution. In contrast, the peaks of the polarization histograms in the planar alignment (i.e. without external field) do not change as a function of depth (Figure 5.4, left column). This suggests that planar alignment is homogeneous independent of depth, which confirms that our LC device consists of a single domain nematic LC.[118] In addition, the absence of a change in the polarization distributions as a function of Z in the absence of an applied E-field also confirms that the LC birefringence has no effect on the fluorescence polarization in our experiments.

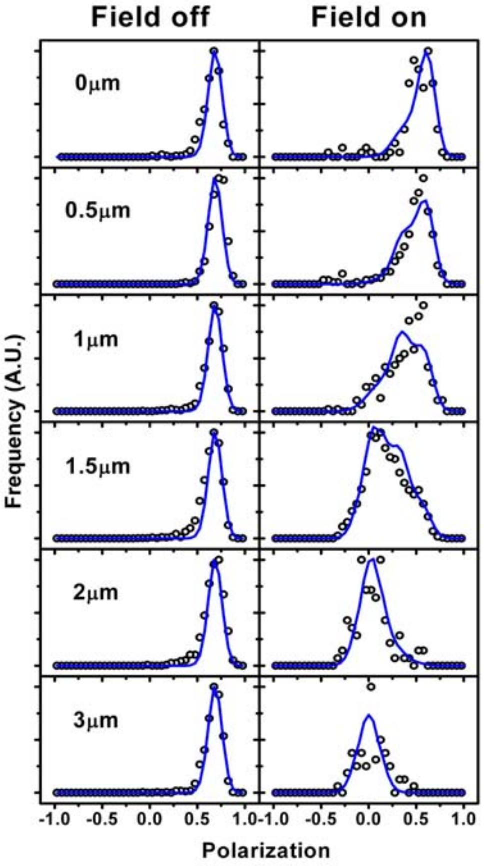

Figure 5.4 Polarization histograms measured using circularly polarized excitation with field off (left column, scatter) and field on (right column, scatter). The laser was focused at different distances from LC-PVA interface, *Z* = 0, 0.5, 1, 1.5, 2, and 3 μm. The simulated polarization histograms (blue lines) for an applied E-field are modeled taking into account the depth dependent of the LC director orientation near the substrate interface based on an elastic model (see Figure 5-5 and text for details).

The spatial director profile of the LC molecules with an external field is usually evaluated using Frank continuum theory,[46,47] where the deformation of the LC is described by a continuous elastic theory, considering the free energy of deformation of the LC and the effect of an electric field. When applying an external field of sufficient magnitude, the LC molecules form two structures, (1) a transition layer in which the LC director changes orientation continuously and (2) a bulk region where the director is perpendicular to the substrate.[47] Figure 5.5 shows the director profile as a function of depth from the interface calculated from Franck continuum theory. The tilt angle θ in Figure 5.5 is the angle between the LC director and the substrate. In the simulation, we choose the *x-y* plane as the substrate surface, the *y*-axis as the nematic director without applying an E-field (i.e. the rubbing direction of alignment layer), and the *z*-axis as the direction of the applied E-field. It is further assumed that the surface anchoring energy is so strong that the tilt angle of the LC molecules at the cell surface is always 0° regardless of the magnitude of the E-field. For the Frank continuum theory, the free energy density of elastic deformation (f_d) and electric field (f_e) are given as:

$$f_d = \frac{1}{2}K_{11}(\nabla\cdot\hat{n})^2 + \frac{1}{2}K_{33}\{\hat{n}\times(\nabla\times\hat{n})\}^2 \tag{5-1}$$

$$f_e = \frac{1}{2}\varepsilon_0\varepsilon_a(\vec{E}\cdot\hat{n})^2 \tag{5-2}$$

K_{11} and K_{33} are the elastic constants for splay and bend deformation, $\hat{n}$ is the unit vector of the nematic director, ε_0 is the dielectric constant in vacuum, and ε_a is the difference of the dielectric constants along and normal to the nematic director. With $(n_y, n_z) = (\cos\theta(z), \sin\theta(z))$ and $\vec{E}\cdot\hat{n} = E\sin\theta$, the total free energy F_t is given by:

$$F_t = \int_0^d \frac{1}{2}\{(K_{11}\cos^2\theta(z) + K_{33}\sin^2\theta(z))(\frac{d\theta(z)}{dz})^2 - \varepsilon_0\varepsilon_a E^2 \sin^2\theta(z)\}dz \qquad (5\text{-}3)$$

where d is the thickness of the cell. The director profile is obtained by minimizing F_t as a function θ using on an iterative finite-difference method.[119] The result for an E-field of ~ 5.5*10^3 V/cm applied to a 5CB nematic device with a thickness of 12.7 μm is shown in Figure 5.

Using the director profile shown in Figure 5.5, obtained from Frank continuum theory, we simulate the polarization histogram for MEH-PPV in 5CB as a function of distance from the LC device interface. For the simulation, it is assumed that the LC device is divided into 127 layers with a thickness of 0.1 μm. In each layer the director orientation is assumed to be constant. The polarization histogram in a single layer is simulated for the same polymer conformation as above (i.e. S_c = 0.70) aligned in the microscope plane and then rotated to match the director orientation in that specific layer. The total polarization histogram in the focal volume with a height of 2.2 μm is obtained using:

$$P_{total}(a) = N(C\sum_{n=0}^{9} Exp(-\frac{2(0.1n-a)^2}{1.1^2})P(0.1n) + \sum_{n=10}^{127} Exp(-\frac{2(0.1n-a)^2}{1.1^2})P(0.1n)) \qquad (5\text{-}4)$$

$P_{total}(a)$ is the total polarization distribution collected from MEH-PPV molecules in the focal volume of a Gaussian beam focused at a depth of a μm. $P(0.1n)$ is the polarization distribution of a single layer at a depth of 0.1n μm. N is the normalization factor and C = 5 is the correction factor for the detection sensitivity.[120] The simulated polarization histograms are shown as blue lines in the right column of Figure 5.4. The simulated (line) and measured (scatter) polarization distributions agree very well and demonstrate that the

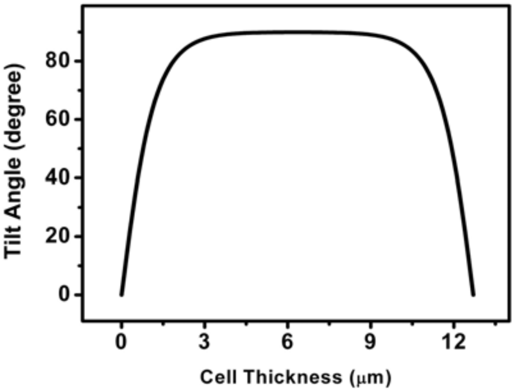

Figure 5.5 Tilt angle distribution as a function of distance from the PVA-LC interface calculated from Frank continuum theory

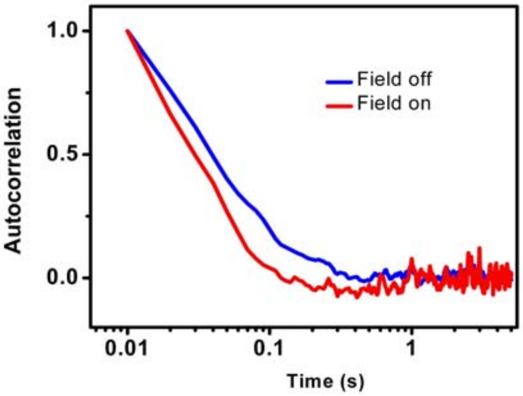

Figure 5.6 Autocorrelation function of MEH-PPV diffusing in 5CB measured at $Z = 0.5\mu m$ with (red) and without (blue) an applied E-field.

MEH-PPV molecules follow the orientation of the LC director as expected from our discussion above, and that the director profile is correctly modeled by Franck continuum theory. MEH-PPV therefore acts as a probe of the local structure in our LC devices and can possibly be used to explore more complex anisotropic media.

It is interesting to compare the diffusion of MEH-PPV near the surface for the E-field switched on vs. switched off. Figure 5.6 shows the autocorrelation of MEH-PPV in 5CB with field off (blue) and field on (red) at $Z = 0.5$ μm. The autocorrelation function is calculated from the MEH-PPV molecules that show a polarization larger than 0.2, i.e. only molecules that are not aligned perfectly perpendicular to the substrate are included. In Figure 5.6 the autocorrelation function with the E-field switched on shows a faster decay than the one with the E-field switched off, suggesting a shorter diffusion time for the MEH-PPV molecules diffusing through the focal volume when an E-field is applied. It has been reported that the viscosity of 5CB is increased near the substrate interface with an applied E-field.[121,122] However, an increase in the local viscosity would imply a slower diffusion of the MEH-PPV molecules, which is contradictory to our observation. Changes in the autocorrelation due to interface-induced quenching of the MEH-PPV can also be ruled out by comparing the fluorescence intensity histograms measured for different focal positions Z and with the field on vs. field off.

Another possible explanation is a change in the “effective focal volume” causing the apparent diffusion time to be faster. None of our experiments suggest that the actual laser focal volume is much smaller with an applied E-field (ignoring small changes due to orientation dependent LC refractive indices). However, the polymer molecules that are orientated perpendicular to the substrate are less likely to be excited because with increasing distance away from the LC device interface, their absorption dipole moments are tilted towards the laser light propagation direction. When the MEH-PPV molecules diffuse vertically away from the substrate into the bulk solvent region while an E-field is applied, they change orientation from a mainly planar alignment with a large absorption probability to a homeotropic alignment with a much smaller absorption probability. The further the MEH-PPV molecules diffuse away from the interface the smaller their contribution to the autocorrelation signal becomes because of a smaller absorption probability. Without an applied field, the MEH-PPV molecules give rise to the same absorption probability even if they diffuse vertically. As a result, the autocorrelation samples a smaller effective region with an applied E-field resulting in a shorter diffusion time as shown in Figure 6. When the E-field is turned on, the effective focal volume for $Z = 0.5$ μm decreases because of the smaller apparent depth in the z-axis. Consistent with this explanation is also the fact that, independent of an applied E-field, no change in the autocorrelation function is observed at $Z = 3$ μm with a diffusion time comparable to the measurement at $Z = 0.5$ μm without an E-field.

Based on the diffusion analysis, the measurable depth in the z-axis is 617±217 nm assuming no change in diffusion constant for MEH-PPV. In the autocorrelation measurement, we select molecules with polarization values larger than 0.2 corresponding to a molecular tilt angle smaller than 51°.For the simulated tilt angle distribution in Figure 5, molecules within 800 nm from the LC substrate interface have tilt angles smaller than 51°. The diffusion analysis is therefore also consistent with the Frank continuum theory.

5.3 CONCLUSION

We have investigated the alignment of a polymer solute with respect to the liquid crystal (LC) director in a LC device while applying an external electric field. The experiments demonstrate that with an external E-field of $5.5*10^3$ V/cm the MEH-PPV molecules are aligned perpendicular to the device substrate in the bulk of the LC without a change of polymer conformation. These results are consistent with our previous model of cooperative anisotropic solvation that describes the high degree of solute alignment with respect to the LC director for the long, stiff MEH-PPV polymer chains in an anisotropic solvent. The E-field studies further imply that it is possible to switch the MEH-PPV alignment by controlling the direction of the anisotropic solvation potential through an E-field. The observed variation of the polarization histogram with distance away from the device interface results from a continuous field-induced deformation of the LC director near the device interface and can be described by a conventional elastic model. The depth-dependent orientation of the MEH-PPV quantitatively matches the director profile that was obtained independently by Frank continuum theory. These results therefore suggest that MEH-PPV can be used as a probe to unveil the complex local structure in a LC.

Chapter 6: Anisotropic Diffusion of Elongated and Aligned Polymer Chains in a Nematic Solvent

6.1 INTRODUCTION

The anisotropic translational diffusion of molecules in anisotropic environments is of growing experimental and theoretical interest.[123-129] A particularly well defined model system is a single-domain, thermotropic nematic liquid crystal (LC), containing a dilute "probe" solute.[124,130-132] Diffusion anisotropy in this cylindrically symmetric system is quantified by the ratio of probe diffusion constant parallel and perpendicular to the nematic director, i.e. $D_{\|}/D_{\perp}$. Various theoretical models[129,133-136] have been developed for $D_{\|}/D_{\perp}$ as a function of the order parameter S in the nematic LC phase. Since the viscosity of the nematic solvent is itself anisotropic, the diffusion of even spherical solutes is moderately anisotropic, e.g. $D_{\|}/D_{\perp} \sim 1.6$ for spheres in a nematic liquid crystal.[123] Experimental results on the diffusion anisotropy of solutes in common thermotropic nematic LCs reveal a broad range of $D_{\|}/D_{\perp}$ values.[124,130-132] For fluorescence probe solutes of comparable size as the LC solvent molecules, $D_{\|}/D_{\perp}$ values ranging from ~ 1.1-4 have been observed, using fluorescence correlation spectroscopy,[124] forced Rayleigh scattering,[130-132] and fluorescence photobleaching recovery spectroscopy.[137]

Theory predicts even larger $D_{\|}/D_{\perp}$ values[134-136] for the *self-diffusion* of highly ordered (macro-)molecules with large aspect ratios due, qualitatively, to the combined effect of the anisotropy of the translational friction of such a rod-like molecules and the tendency for rod-like molecules to be highly aligned in the nematic LC phase. This was just recently confirmed for the self-diffusion of the colloidal rod-like virus *fd*, which has an aspect ratio greater than 100 and forms a lyotropic LC at high concentrations.[138] By video imaging of individual dye-labeled *fd* virus molecules dissolved in a background of non-labeled viruses, diffusion anisotropies $D_{\parallel}/D_{\perp}$ ranging from 7.5 to >20 were determined in the nematic phase as a function of increasing order parameter. This work addresses the question: What is the diffusion anisotropy of a highly aligned and elongated probe dissolved in the nematic phase of a low molecular weight LC solvent?

In this work, the directional diffusion constant of a fluorescent probe molecule is determined from the intensity cross-correlation of fluorescence originating from the same molecule diffusing through two spatially separated probe volumes. A new chopping/synchronous-detection scheme is employed to reject a serious cross-talk background in the data. The probe molecule used in this study is the rod-like conjugated polymer MEH-PPV, and the solvent is the thermotropic LC 5CB. We have recently shown that MEH-PPV molecules are highly aligned in 5CB, with an order parameter, $S = \frac{1}{2}\left\langle 3\cos^2\alpha - 1 \right\rangle$, of 0.99 compared to 0.48 for 5CB,[87] where α is the angle between the long axis of the MEH-PPV molecule and the LC director.[57,83] In addition, recent results have shown that the conformation of MEH-PPV is elongated along the director.[57] With information on the shape of the probe molecules we are able in this work to make predictions for $D_{\parallel}/D_{\perp}$ and compare the predicted values to the experimental value obtaining new insights on the anisotropy of molecular diffusion in an anisotropic environment. Our main conclusion is that the translational dynamics of the solute is primarily governed by the nematic order of the solvent.

6.2 RESULTS AND DISCUSSION

The chopping scheme described in chapter 2.2.4 is crucial for eliminating background and makes the cross-correlation measurement feasible. Figure 6.1A shows dual-channel fluorescence intensity transients from MEH-PPV in 5CB with overlapping focal volumes, i.e. $r = 0$ μm. The individual blips correspond to single molecules passing through the two focal volumes, which in this case are overlapped. The intensity for the two channels is plotted in opposite vertical directions in the plot in order to make the individual transients easier to visualize. The analogous transients recorded with either one or the other laser beams blocked are shown in Figures 6.1B and C, respectively. These data demonstrate that the chopping/synchronous detection scheme (described in chapter 2.2.4) completely suppresses the cross-talk originating from the opposite probe volume, even at $r = 0$ μm focal volume separation. Without the chopping/synchronous detection scheme, cross-talk due to overlapping focal volumes (which includes diffraction rings) is a large background, and major complication for the cross-correlation measurement. Our setup is therefore a significant improvement over a previously described two-beam cross-correlation technique that did not employ chopping.[139]

Diffusion constants are obtained by fitting the fluorescence cross-correlation $G_c(\tau)$, obtained from the intensity transients, *F(t),* to a model. *F(t)* is acquired with a bin time of 10 ms. We acquire data for periods up to several hours, which is necessary to

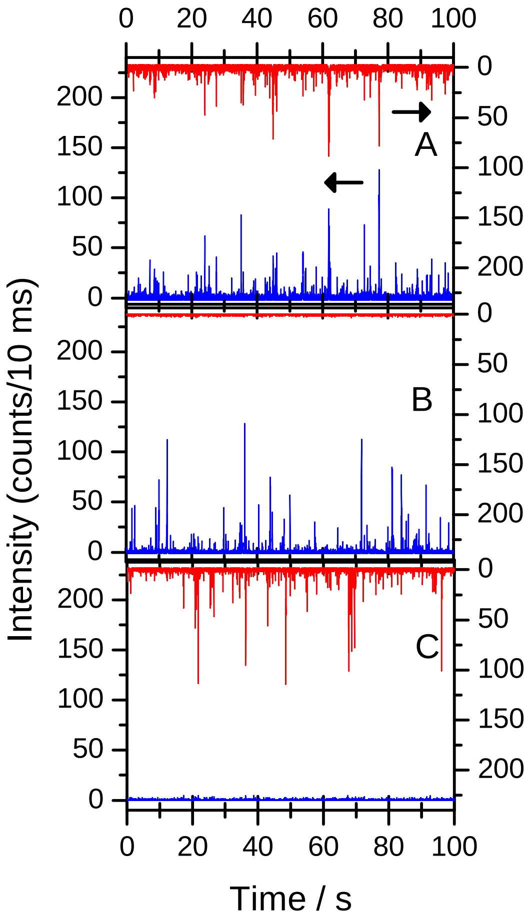

Figure 6.1 Dual-channel fluorescence transients from MEH-PPV in 5CB for a beam separation of 0 µm. Part A shows the raw signal with both beams on while parts B and C were recorded with either laser beam blocked. This illustrates complete suppression of cross-talk originating from the opposite probe volume even at 0 µm beam separation.

achieve an adequate signal-to-noise, especially for the large beam separations, since the cross-correlation amplitude rapidly decays with distance. The fluorescence cross-correlation $G_c(\tau)$ is obtained from the analysis of *F(t)*,as follows:[140]

$$G_c(\tau) = \frac{< \delta F_1(t) \cdot \delta F_2(t+\tau) >}{< F_1(t) > \cdot < F_2(t) >} \tag{6-1}$$

Here τ is the lag time, $F_1(t)$ and $F_2(t)$ are the fluorescence intensities measured by the two detectors, and the brackets denote time-averaged values.

In order to increase the signal to noise ratio of the $G_c(\tau)$, intensity bursts in *F(t)* are first subjected to a threshold condition allowing us to remove unwanted signal from smaller MEH-PPV molecules and background counts from 5CB. The experimental results for MEH-PPV diffusing in 5CB are shown in Figure 6.2 for beam separations corresponding to a 0 μm (essentially an autocorrelation, top), 1 μm (middle), and 2 μm (bottom). The lines through the data are fits for the focal volume separation axis parallel (blue) and perpendicular (red) to the LC director. The $G_c(\tau)$ at a beam separation of 2 μm shows a pronounced anticoincidence at early times consistent with the fact that the same molecule cannot be present in both detection volumes at the same time.

The $G_c(\tau)$ data are analyzed employing an analytical model that is closely analogous to previous reports.[139-141] The model is based on the assumptions that the fluorescence intensity fluctuation is due only to concentration fluctuations of the MEH-PPV, the focal spots have a 3-D Gaussian beam profile, and the concentration of MEH-PPV follows a Poisson distribution. This leads to the following expression of $G_c(\tau)$ for molecules diffusing between the two detection volumes:

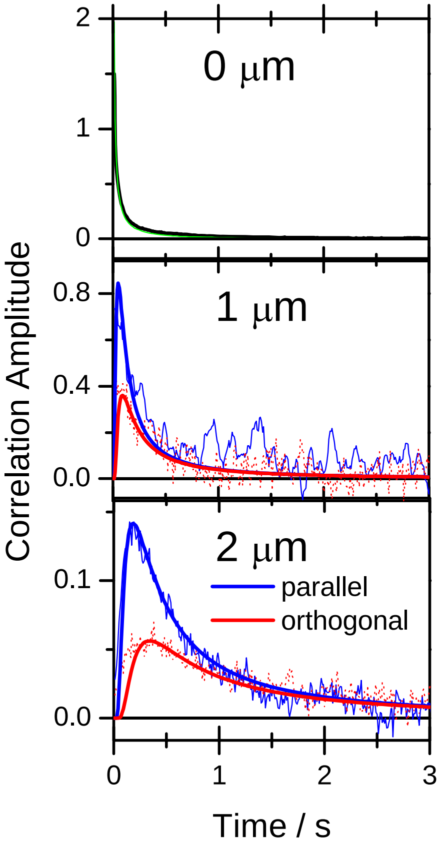

Figure 6.2 Autocorrelation (top, 0 μm) and two-beam cross-correlations at beam separations of 1 μm (middle) and 2 μm (bottom) for MEH-PPV diffusing in 5CB. For both beam separations the cross-correlations were fitted (solid lines) according to equation (2) with diffusion constants of $D_{\parallel}$ = (3.8±0.5)*10^{-12} m^2 s^{-1} and $D_{\perp}$ = (2.0±0.5)*10^{-12} m^2s^{-1} for parallel (blue) and perpendicular (red) diffusion with respect to the LC director. The autocorrelation was calculated using the isotropic average, i.e. $\langle D \rangle = (D_{\parallel} + 2D_{\perp})/3$ = (2.6±0.5)*10^{-12} m^2 s^{-1}

$$G_c^{\,x,y}(\tau) = \frac{1}{<C> \pi \sqrt{4D_x\tau + w_0^2}\sqrt{4D_y\tau + w_0^2}\sqrt{4D_z\tau + z_0^2}} e^{-\frac{r^2}{4D_{x,y}\tau + w_0^2}} \qquad (6\text{-}2)$$

<*C*> is the mean concentration of MEH-PPV, w_0 is the 1/e^2 radius of the Gaussian beam in the sample plane (xy), $2z_o$ is the height of the focal volume, and r is the distance between the two laser spots. $G_c^{\,x}(\tau)$ and $G_c^{\,y}(\tau)$ correspond to diffusion parallel and perpendicular to the LC director. Values of w_0 = 100 nm and z_0/w_0 = 5 were used in the analysis.

The solid lines in Figure 6.2 are best-fits of the data using equation (6-2), and agree well with the experimental results. The fit procedure involved first fitting the autocorrelation data (Figure 3A) using an isotropic diffusion constant, i.e. $<D> = (D_{\|} + 2D_{\perp})/3$, and then using <*D*> as a constraint for the data with beam separations of 1 and 2 μm. However, a 3 parameter global fit gives similar results. From the best-fit parameters, we obtained $D_x = D_{\|} = (3.8\pm0.5)*10^{-12}$ m^2 s^{-1} and $D_z = D_y = D_{\perp} = (2.0\pm0.5)*10^{-12}$ m^{2}s^{-1}. The excellent agreement between experiment and predicted curves supports the validity of the overall method of analysis. Finally, using the best-fit values a diffusion anisotropy ratio $D_{\|}/D_{\perp} = 1.9 \pm 0.3$ can be determined for MEH-PPV in 5CB.

There are two sources of diffusion anisotropy for solutes in liquid crystalline solvents. The first is the anisotropy of the solute itself and the second is the anisotropy in the friction between the solute and the solvent. Consider, for example, the dynamics of a rod-like molecule. Physically, one expects its diffusion in the direction along its axis to be less hindered than in the direction perpendicular to its axis. In a dilute solute of rods in an isotropic solvent, for example, one has $D_{\|}/D_{\perp} = 2$.[142] The anisotropy of the friction with the solvent can also induce an anisotropic diffusion because the solvent friction is lower along the nematic director, and for a sphere in a nematic solvent, $D_{\|}/D_{\perp} \sim 1.6$.[123,6] One might therefore expect $D_{\|}/D_{\perp} > 2$ for rods in a nematic solvent.

Most theories have addressed the self-diffusion of anisotropic molecules in the nematic phase. For very long rods in semi-dilute *isotropic* solutions, $D_{\perp} \sim 0$ and the diffusion anisotropy is infinite. For the self-diffusion in the nematic phase a number of models that have been proposed. Models by Hess, Frenkel and Allen (HFA)[136] and by Chu and Moroi (CM)[135] for the self-diffusion of nematic LCs predict that the molecular diffusion anisotropy strongly increases with increasing order parameter S and aspect ratio e. In these models, the diffusion anisotropy becomes *independent* of e for large e, and in the asymptotic limit of infinite e, $D_{\|}/D_{\perp} = (1 + 2S)/(1 - S) = 3.8$ for $S = 0.48$. Computer simulations of hard spherocylinders[134] have confirmed this prediction as an upper bound to the anisotropy and also demonstrated that $D_{\|}/D_{\perp}$ is independent of e over the range ($4 \leq e \leq 16$) they studied. For $S = 0.48$, the simulations find that $D_{\|}/D_{\perp} \sim 2 - 2.5$, independent of e. A diffusion anisotropy of 1.9 ± 0.3 is surprisingly small in light of the high orientational anisotropy of the MEH-PPV chains and the fact that for the self-diffusion of 5CB $D_{\|}/D_{\perp} = 2.7$.[130,131,143,144]

It is of interest to adapt the models for the self-diffusion of nematic LCs to the tracer diffusion of solutes in nematic solvents. The two parameters in the models are the aspect ratio of the molecules and the nematic order parameter. For MEH-PPV in 5CB, the solute order parameter is $S = 0.99$,[57] and using this value in the models gives diffusion anisotropies that are far too large, i.e., 65.8 and 11.2, respectively, in the HFA and CM theories (see Table 6.1). We therefore conclude that the appropriate order parameter in the models is that of the solvent, and this gives diffusion anisotropies of 3.6 and 3.1, respectively, for the HFA and CM theories, for S = 0.48.[87] This is in much better agreement with experiment, although the models significantly overestimate the anisotropy measured in experiment.

Extensions of the hydrodynamic theory by Kirkwood and Riseman (KR)[145] to our system using the anisotropy of the solvent viscosity ($\eta_{\|}/\eta_{\perp}$ = 1.7)[6] give predictions in reasonable accord with our experiments. In order to account for the non-spherical shape of MEH-PPV, we compute the diffusion constants of a cylindrically shaped polymer with length L and aspect ratio e according to a hydrodynamic model by Garcia de la Torre (GT) and coworkers.[146-148] For cylinders, the *intrinsic molecular diffusion anisotropy* in dilute (isotropic) solutions increases slowly with increasing aspect ratio. In case of the modeled conformation of our MEH-PPV sample the intrinsic diffusion anisotropy is 1.4 for an aspect ratio of 9.2. The experimentally observed diffusion anisotropy for a cylinder in a LC solvent is then the product of the intrinsic diffusion anisotropy and the anisotropy of the solvent viscosity yielding a diffusion anisotropy of 2.4, which is in reasonable agreement with our measurements. The predictions of various theories for the diffusion anisotropy are collected in Table 1, where the solute geometric parameters are obtained from a previously modeled[57] MEH-PPV conformation.The experiments shed light on the hydrodynamic boundary conditions for solute diffusion in nematic solvents. The anistropic diffusion of rods is qualitatively different for stick and slip boundary conditions. In the case of stick, the friction scales with the length of the rod in both the parallel and perpendicular directions, and the diffusion

Table 6.1:

A comparison of experimental and theoretical results for the anisotropy ratio $D_\parallel/D_\perp$ for MEH-PPV in 5CB.

Model / Reference [#]	$\boldsymbol{D_\parallel/D_\perp}$	**Equations**
Experiment	1.9	
Hess, Frenkel, Allen (HFA) $S = 0.48\ (0.99)$, $e = 9.2$ [13]	3.6 (65.8)	$D_\parallel = <D>_g \kappa[e^{4/3} - 2e^{-2/3}(e^2-1)(1-S)/3]$ $D_\perp = <D>_g \kappa[e^{-2/3} - 2e^{-2/3}(e^2-1)(1-S)/3]$
Chu and Moroi (CM) $S = 0.48\ (0.99)$, $e = 9.2$ [14]	3.1 (11.2)	$D_\parallel = <D> (1 + \frac{2-2\pi/4e}{1+2\pi/4e} S)$ $D_\perp = <D> (1 - \frac{1-\pi/4e}{1+2\pi/4e} S)$
Kirkwood-Riseman (KR) $R_G = 30.0$ nm [27]	1.7	$D_\parallel = \frac{4kT}{9\pi^2 \eta_\parallel R_G}$ $D_\perp = \frac{4kT}{9\pi^2 \eta_\perp R_G}$
Garcia de la Torre (GT) Cylinders/Ellipsoids (Stick boundary cond.), $L = 88.8$ nm, $e = 9.2$ [28-30]	2.4	$D_\parallel = \frac{kT}{2\pi\eta_\parallel L}(\ln e + \nu_\parallel)$ $D_\perp = \frac{kT}{4\pi\eta_\perp L}(\ln e + \nu_\perp)$
Tang and Evans (TE) / Allison Ellipsoids (Slip boundary cond.), $L = 88.8$ nm, $e = 9.2$ [31,32]	9.2 / 6.9	Calculated with numerical values for D_{slip}/D_{stick} according to TE / Allison

The polymer dimensions were calculated from conformations obtained by Monte Carlo simulations of 100 beads representing 250 repeat units and having 15 defects in a LC solvation potential[57] and were scaled up to the molecular weight (MW) of the experimental sample according to $MW^{3/5}$.

$<D>_g = (D_\parallel^{1/3} * D_\perp^{2/3})$ is the geometric average for the isotropic diffusion constant.

$\kappa = [1+2(e^{-2}-1)(1-S)/3]^{-1/3} \cdot [1+(e^2-1)(1-S)/3]^{-2/3}$

k = Boltzmann constant, T = temperature, R_G = radius of gyration

$\nu_\parallel$ and $\nu_\perp$ are end-effect correction factors and are functions of the aspect ratio e. For all other definitions refer to the text.

anisotropy becomes independent of the aspect ratio in the limit of large e. In the case of slip, however, the friction in the direction parallel to the rod axis is independent of the aspect ratio and the anisotropy becomes an increasing function of the length of the rod. The small value of the diffusion anisotropy for $e = 9.2$ suggests that stick boundary conditions are more appropriate for polymers in a nematic solvent. This conclusion can be made more quantitative by comparing to numerical solutions for hard ellipsoids.[149,150] If we use our estimated aspect ratio and calculate the diffusion anisotropy based on slip boundary conditions using the numerical results of Tang and Evans (TE)[149] and Allison,[150] respectively, we obtain values of $D_{\|}/D_{\perp} = 9.2$ and 6.9, which is much larger than the anisotropy measured. We therefore conclude that stick is the more appropriate boundary condition for this system.

It is worth to briefly discuss why the observed diffusion anisotropy for MEH-PPV is smaller than the values predicted by theory and also smaller compared to the anisotropy of perylene in a nematic LC mixture measured by a similar fluorescence correlation technique ($D_{\|}/D_{\perp} = 4.0$),[2] as well the anisotropy for the solvent self-diffusion ($D_{\|}/D_{\perp} = 2.7$).[130,131,143,144] In the calculations, we have neglected the effect of the polymer solute on the intrinsic solvent viscosity. An increase in the viscosity might have a larger effect on the diffusion parallel to the long polymer axis, thus reducing the observed diffusion anisotropy. This could qualitatively be rationalized in the following way. The friction for the parallel motion of the polymer is enhanced due to the segmented nature of the polymer chain. Because of defects along the polymer chain, our MEH-PPV sample typically consists of about 8-10 segments despite the rigid nature of the conjugated backbone. If the diffusion of an individual segment is similar to the solvent, then one would expect that for the linked segments in a stretched polymer chain the parallel diffusion is hindered as the segments tend to run into each other more frequently in the parallel direction. On the other hand, the large size of the polymer compared to the solvent makes the chain sample the solvent much more than shorter molecules, which has the effect of reducing the diffusion anisotropy to that of a sphere.

6.3 CONCLUSION

The translational diffusion constant of a polymer *solute* in a single nematic LC (5CB) *solvent*, is measured for directions parallel and perpendicular to the LC director (i.e. $D_\|$ and $D_\perp$, respectively), using a fluorescence two-beam, cross-correlation technique. The solute under investigation is the stiff, conjugated polymer, MEH-PPV. The diffusional anisotropy ratio $D_\|/D_\perp$ is observed to be 1.9 ± 0.3, which is surprisingly small since MEH-PPV is known to be both elongated and highly aligned along the LC director of 5CB due to cooperative solvation along the polymer chain. These results suggest that the diffusional anisotropy of macromolecules in anisotropic media is rather insensitive to the solute's alignment and conformation, but is mainly dominated by the properties of the solvent.

REFERENCE

(1) Wang, H. L.; MacDiarmid, A. G.; Wang, Y. Z.; Gebler, D. D.; Epstein, A. J. *Synthetic Met* **1996**, *78*, 33.

(2) Hide, F.; DiazGarcia, M. A.; Schwartz, B. J.; Heeger, A. J. *Accounts Chem Res* **1997**, *30*, 430.

(3) Friend, R. H.; Gymer, R. W.; Holmes, A. B.; Burroughes, J. H.; Marks, R. N.; Taliani, C.; Bradley, D. D. C.; Dos Santos, D. A.; Bredas, J. L.; Logdlund, M.; Salaneck, W. R. *Nature* **1999**, *397*, 121.

(4) Nguyen, T.-Q.; Wu, J.; Doan, V.; Schwartz, B. J.; Tolbert, S. H. *Science* **2000**, *288*, 652.

(5) Mehta, A.; Kumar, P.; Dadmun, M. D.; Zheng, J.; Dickson, R. M.; Thundat, T.; Sumpter, B. G.; Barnes, M. D. *Nano Lett.* **2003**, *3*, 603.

(6) Huser, T.; Yan, M.; Rothberg, L. J. *P. Natl. Acad. Sci. USA* **2000**, *97*, 11187.

(7) Hu, D. H.; Yu, J.; Wong, K.; Bagchi, B.; Rossky, P. J.; Barbara, P. F. *Nature* **2000**, *405*, 1030.

(8) Hu, D. H.; Yu, J.; Padmanaban, G.; Ramakrishnan, S.; Barbara, P. F. *Nano Lett.* **2002**, *2*, 1121.

(9) Barbara, P. F.; Gesquiere, A. J.; Park, S.-J.; Lee, Y. J. *Acc. Chem. Res.* **2005**, *38*, 602.

(10) Yu, J.; Hu, D. H.; Barbara, P. F. *Science* **2000**, *289*, 1327.

(11) Kang, S. W.; Jin, S. H.; Chien, L. C.; Sprunt, S. *Adv. Funct. Mater.* **2004**, *14*, 329.

(12) Hulvat, J. F.; Stupp, S. I. *Angew. Chem., Int. Ed.* **2003**, *42*, 778.

(13) Hulvat, J. F.; Stupp, S. I. *Adv. Mater.* **2004**, *16*, 589.

(14) Hatano, T.; Bae, A. H.; Takeuchi, M.; Fujita, N.; Kaneko, K.; Ihara, H.; Takafuji, M.; Shinkai, S. *Angew. Chem., Int. Ed.* **2004**, *43*, 465.

(15) Kumar, P.; Mehta, A.; Dadmun, M. D.; Zheng, J.; Peyser, L.; Bartko, A. P.; Dickson, R. M.; Thundat, T.; Sumpter, B. G.; Noid, D. W.; Barnes, M. D. *J. Phys. Chem. B* **2003**, *107*, 6252.

(16) Hu, D. H.; Yu, J.; Padmanaban, G.; Ramakrishnan, S.; Barbara, P. F. *Nano Lett.* **2002**, *2*, 1121.

(17) Huser, T.; Yan, M. *J. Photochem. Photobiol., A* **2001**, *144*, 43.

(18) Huser, T.; Yan, M.; Rothberg, L. J. *Proc. Natl. Acad. Sci. U. S. A.* **2000**, *97*, 11187.

(19) Acharya, B. R.; Primak, A.; Kumar, S. *Phys Rev Lett* **2004**, *92*.

(20) Chigrinov, V. G. *Liquid Crystal Device, Physics and Applications*; Artech House, 1999.

(21) D. Demus, J. G., G.W. Gray, H.-W. Spiess, V. Vill *Physical Properties of Liquid Crystals*; Wiley-Vch, 1999.

(22) de Gennes, P.-G.; Frost, J. *The Physics of Liquid Crystals*; Clarendon Press: Oxford, U.K., 1993.

(23) Leadbetter, A. J.; Durrant, J. L. A.; Rugman, M. *Mol Cryst Liq Cryst* **1977**, *34*, 231.

(24) Ekgasit, S.; Fulleborn, M.; Siesler, H. W. *Vibrational Spectroscopy* **1999**, *19*, 85.

(25) Fukazawa, T.; Tadokoro, T.; Toriumi, H.; Akahane, T.; Kimura, M. *Thin Solid Films* **1998**, *313*, 799.

(26) Mitsuishi, M.; Ito, S.; Yamamoto, M.; Fischer, T.; Knoll, W. *Journal of Applied Physics* **1997**, *81*, 1135.

(27) Noble, A. R.; Kwon, H. J.; Nuzzo, R. G. *Journal of the American Chemical Society* **2002**, *124*, 15020.

(28) Noble-Luginbuhl, A. R.; Blanchard, R. M.; Nuzzo, R. G. *Journal of the American Chemical Society* **2000**, *122*, 3917.

(29) Okutani, S.; Kimura, M.; Toriumi, H.; Akao, K.; Tadokoro, T.; Akahane, T. *Japanese Journal of Applied Physics Part 1-Regular Papers Short Notes & Review Papers* **2001**, *40*, 244.

(30) Shilov, S. V.; Okretic, S.; Siesler, H. W. *Vibrational Spectroscopy* **1995**, *9*, 57.

(31) Smith, N. J.; Sambles, J. R. *Applied Physics Letters* **2000**, *77*, 2632.

(32) Smith, N. J.; Tillin, M. D.; Sambles, J. R. *Physical Review Letters* **2002**, *88*.

(33) Tadokoro, T.; Fukazawa, T.; Toriumi, H. *Japanese Journal of Applied Physics Part 2-Letters* **1997**, *36*, L1207.

(34) Tadokoro, T.; Toriumi, H.; Okutani, S.; Kimura, M.; Akahane, T. *Japanese Journal of Applied Physics Part 1-Regular Papers Short Notes & Review Papers* **2003**, *42*, 4552.

(35) Toriumi, H.; Akahane, T. *Japanese Journal of Applied Physics Part 1-Regular Papers Short Notes & Review Papers* **1998**, *37*, 608.

(36) Yang, F. Z.; Ruan, L. Z.; Sambles, J. R. *Journal of Applied Physics* **2000**, *88*, 6175.

(37) Yang, C. L.; Chen, S. H. *Japanese Journal of Applied Physics, Part 1: Regular Papers, Brief Communications & Review Papers* **2002**, *41*, 3778.

(38) Smalyukh, II; Shiyanovskii, S. V.; Lavrentovich, O. D. *Chemical Physics Letters* **2001**, *336*, 88.

(39) Lavrentovich, O. D. *Pramana-Journal of Physics* **2003**, *61*, 373.

(40) Gheorghiu, N.; Smalyukh, II; Lavrentovich, O. D.; Gleeson, J. T. *Physical Review E* **2006**, *74*.

(41) Dierking, I. *Chemphyschem* **2001**, *2*, 663.

(42) Ozaki, R.; Aoki, M.; Moritake, H.; Yoshino, K.; Toda, K. *Japanese Journal of Applied Physics, Part 1: Regular Papers, Brief Communications & Review Papers* **2006**, *45*, 4662.

(43) Moritake, H.; Kim, J.; Toda, K.; Yoshino, K. *Molecular Crystals and Liquid Crystals* **2005**, *436*, 1201.

(44) Moritake, H.; Kim, J.; Yoshino, K.; Toda, K. *Japanese Journal of Applied Physics, Part 1: Regular Papers, Brief Communications & Review Papers* **2005**, *44*, 4316.

(45) Moritake, H.; Kim, J.; Yoshino, K.; Toda, K. *Japanese Journal of Applied Physics, Part 1: Regular Papers, Brief Communications & Review Papers* **2004**, *43*, 6780.

(46) Frank, F. C. *Discussions of the Faraday Society* **1958**, *29*, 19.

(47) de Gennes, P. G. a. P., J *The physics of Liquid Crystal*, 2nd ed.; Oxford Science Publications, 1993.

(48) De Gennes, P. G. *The physics of liquid crystal*; Oxford University Press, 1974.

(49) Itou, T.; Teramoto, A. *Macromolecules* **1984**, *17*, 1419.

(50) Adams, M.; Dogic, Z.; Keller, S. L.; Fraden, S. *Nature* **1998**, *393*, 349.

(51) Islam, M. F.; Alsayed, A. M.; Dogic, Z.; Zhang, J.; Lubensky, T. C.; Yodh, A. G. *Phys. Rev. Lett.* **2004**, *92*.

(52) Lammi, R. K.; Fritz, K. P.; Scholes, G. D.; Barbara, P. F. *J. Phys. Chem. B* **2004**, *108*, 4593.

(53) Dogic, Z.; Zhang, J.; Lau, A. W. C.; Aranda-Espinoza, H.; Dalhaimer, P.; Discher, D. E.; Janmey, P. A.; Kamien, R. D.; Lubensky, T. C.; Yodh, A. G. *Phys. Rev. Lett.* **2004**, *92*.

(54) Dierking, I.; Scalia, G.; Morales, P.; LeClere, D. *Adv. Mater.* **2004**, *16*, 865.

(55) Link, S.; Hu, D.; Chang, W. S.; Scholes, G. D.; Barbara, P. F. *Nano Letters* **2005**, *5*, 1757.

(56) Link, S.; Chang, W. S.; Yethiraj, A.; Barbara, P. F. *Physical Review Letters* **2006**, *96*.

(57) Link, S.; Hu, D.; Chang, W.-S.; Scholes, G. D.; Barbara, P. F. *Nano Lett.* **2005**, *5*, 1757.

(58) Padmanaban, G.; Ramakrishnan, S. *J. Am. Chem. Soc.* **2000**, *122*, 2244.

(59) Padmanaban, G.; Ramakrishnan, S. *J. Phys. Chem. B* **2004**, *108*, 14933.

(60) Fritz, K. P.; Scholes, G. D. *J. Phys. Chem. B* **2003**, *107*, 10141.

(61) Szabo, A. *J. Chem. Phys.* **1980**, *72*, 4620.

(62) Martynski, T.; Mykowska, E.; Bauman, D. *J. Mol. Struct.* **1994**, *325*, 161.

(63) Chapoy, L. L.; Dupre, D. B. *J. Chem. Phys.* **1978**, *69*, 519.

(64) Chapoy, L. L.; Dupre, D. B. *J. Chem. Phys.* **1979**, *70*, 2550.

(65) Ha, T.; Laurence, T. A.; Chemla, D. S.; Weiss, S. *J. Phys. Chem. B* **1999**, *103*, 6839.

(66) Ha, T.; Glass, J.; Enderle, T.; Chemla, D. S.; Weiss, S. *Phys. Rev. Lett.* **1998**, *80*, 2093.

(67) Woo, H. S.; Lhost, O.; Graham, S. C.; Bradley, D. D. C.; Friend, R. H.; Quattrocchi, C.; Bredas, J. L.; Schenk, R.; Mullen, K. *Synth. Met.* **1993**, *59*, 13.

(68) Pleiner, H. *Mol. Cryst. Liq. Cryst. A* **1997**, *292*, 1.

(69) Axelrod, D. *Biophys. J.* **1979**, *26*, 557.

(70) Forkey, J. N.; Quinlan, M. E.; Goldman, Y. E. *Prog. Biophys. Mol. Bio.* **2000**, *74*, 1.

(71) Peterson, K. A.; Fayer, M. D. *J. Chem. Phys.* **1986**, *85*, 4702.

(72) Aragon, S. R.; Pecora, R. *J. Chem. Phys.* **1976**, *64*, 1791.

(73) Beljonne, D.; Pourtois, G.; Silva, C.; Hennebicq, E.; Herz, L. M.; Friend, R. H.; Scholes, G. D.; Setayesh, S.; Mullen, K.; Bredas, J. L. *Proc. Natl. Acad. Sci. U. S. A.* **2002**, *99*, 10982.

(74) Hu, D. H.; Lu, H. P. *J. Phys. Chem. B* **2003**, *107*, 618.

(75) Stevens, B. C.; Ha, T. *J. Chem. Phys.* **2004**, *120*, 3030.

(76) Yeh, P. G., Claire *Optics of liquid crystal displays*; John Willey &Sons Inc., 1999.

(77) Saleh, B. E. A. T., Malvin Carl *Fundamentals of Photonics*; John Wiley &sons, Inc., 1991.

(78) Gu, C.; Yeh, P. *Displays* **1999**, *20*, 237.

(79) Carmesin, I.; Kremer, K. *Macromolecules* **1988**, *21*, 2819.

(80) Onsager, L. *Ann. N. Y. Acad. Sci.* **1949**, *51*, 627.

(81) Lekkerkerker, H. N. W.; Coulon, P.; Van Der Haegen, R.; Deblieck, R. *J. Chem. Phys.* **1984**, *80*, 3427.

(82) Dogic, Z.; Zhang, J.; Lau, A. W. C.; Aranda-Espinoza, H.; Dalhaimer, P.; Discher, D. E.; Janmey, P. A.; Kamien, R. D.; Lubensky, T. C.; Yodh, A. G. *Phys. Rev. Lett.* **2004**, *92*, 125503.

(83) Lammi, R. K.; Fritz, K. P.; Scholes, G. D.; Barbara, P. F. *J. Phys. Chem. B* **2004**, *108*, 4593.

(84) Padmanaban, G.; Ramakrishnan, S. *J. Am. Chem. Soc.* **2000**, *122*, 2244.

(85) Fritz, K. P.; Scholes, G. D. *J. Phys. Chem. B* **2003**, *107*, 10141.

(86) Woo, H. S.; Lhost, O.; Graham, S. C.; Bradley, D. D. C.; Friend, R. H.; Quattrocchi, C.; Bredas, J. L.; Schenk, R.; Muellen, K. *Synth. Met.* **1993**, *59*, 13.

(87) Salamon, Z.; Skibinski, A. *Mol. Cryst. Liq. Cryst.* **1983**, *90*, 205.

(88) Forkey, J. N.; Quinlan, M. E.; Goldman, Y. E. *Prog. Biophys. Mol. Biol.* **2000**, *74*, 1.

(89) Chang, W.-S.; Link, S.; Hu, D.; Barbara, P. F., to be published.

(90) Szabo, A. *J. Chem. Phys.* **1980**, *72*, 4620.

(91) D'Allest, J. F. D.; Maissa, P.; ten Bosh, A.; Sixou, P.; Blumstein, A.; Blumstein, R.; Teixeira, J.; Noirez, L. *Phys. Rev. Lett.* **1988**, *61*, 2562.

(92) Chen, F.-L.; Jamieson, A. M. *Macromolecules* **1994**, *27*, 4691.

(93) Chiang, Y.-C.; Jamieson, A. M.; Campbell, S.; Tong, T. H.; Sidocky, N. D.; Chien, L. C.; Kawasumi, M.; Percec, V. *Polymer* **2000**, *41*, 4127.

(94) de Gennes, P.-G. *Scaling Concepts in Polymer Physics*; Cornell Univ. Press: Ithaca, New York, 1979.

(95) Ivanov, V. A.; Paul, W.; Binder, K. *J Chem Phys* **1998**, *109*, 5659.

(96) Dallest, J. F.; Maissa, P.; Tenbosch, A.; Sixou, P.; Blumstein, A.; Blumstein, R.; Teixeira, J.; Noirez, L. *Phys Rev Lett* **1988**, *61*, 2562.

(97) Chen, F. L.; Jamieson, A. M. *Macromolecules* **1994**, *27*, 4691.

(98) Dogic, Z.; Zhang, J.; Lau, A. W. C.; Aranda-Espinoza, H.; Dalhaimer, P.; Discher, D. E.; Janmey, P. A.; Kamien, R. D.; Lubensky, T. C.; Yodh, A. G. *Phys Rev Lett* **2004**, *92*, 125503.

(99) Alsnielsen, J.; Birgeneau, R. J.; Kaplan, M.; Litster, J. D.; Safinya, C. R. *Phys Rev Lett* **1977**, *39*, 1668.

(100) Stamatoff, J.; Cladis, P. E.; Guillon, D.; Cross, M. C.; Bilash, T.; Finn, P. *Phys Rev Lett* **1980**, *44*, 1509.

(101) Rieker, T. P.; Janulis, E. P. *Phys Rev E* **1995**, *52*, 2688.

(102) McMillan, W. L. *Phys. Rev. A* **1972**, *6*, 936.

(103) Lansac, Y.; Glaser, M. A.; Clark, N. A.; Lavrentovich, O. D. *Nature* **1999**, *398*, 54.

(104) Maiti, P. K.; Lansac, Y.; Glaser, M. A.; Clark, N. A. *Phys Rev Lett* **2002**, *88*, 65504.

(105) Guymon, C. A.; Hoggan, E. N.; Clark, N. A.; Rieker, T. P.; Walba, D. M.; Bowman, C. N. *Science* **1997**, *275*, 57.

(106) Krentsel, T. A.; Lavrentovich, O. D.; Kumar, S. *Molecular Crystals and Liquid Crystals Science and Technology Section a-Molecular Crystals and Liquid Crystals* **1997**, *304*, 463.

(107) Lafouresse, M. G.; Sied, M. B.; Allouchi, H.; Lopez, D. O.; Salud, J.; Tamarit, J. L. *Chem Phys Lett* **2003**, *376*, 188.

(108) Yethiraj, A.; Bechhoefer, J. *Phys Rev Lett* **2000**, *84*, 3642.

(109) Hoeben, F. J. M.; Jonkheijm, P.; Meijer, E. W.; Schenning, A. *Chemical Reviews* **2005**, *105*, 1491.

(110) Kato, T.; Mizoshita, N.; Kishimoto, K. *Angewandte Chemie-International Edition* **2006**, *45*, 38.

(111) Onsager, L. *Annals of the New York Academy of Sciences* **1949**, *51*, 627.

(112) Boichuk, V.; Kucheev, S.; Parka, J.; Reshetnyak, V.; Reznikov, Y.; Shiyanovskaya, I.; Singer, K. D.; Slussarenko, S. *Journal of Applied Physics* **2001**, *90*, 5963.

(113) Bryan-Brown, G. P.; Wood, E. L.; Sage, I. C. *Nature* **1999**, *399*, 338.

(114) Presnyakov, V. V.; Galstian, T. V. *Journal of Applied Physics* **2005**, *97*.

(115) Sugimura, A.; Ishino, D.; Matsumoto, K.; Ishihara, S. *Molecular Crystals and Liquid Crystals* **2003**, *400*, 97.

(116) Lelidis, I.; Nobili, M.; Durand, G. *Physical Review E* **1993**, *48*, 3818.

(117) Mottram, N. J.; Hogan, S. J. *Continuum Mechanics and Thermodynamics* **2002**, *14*, 281.

(118) Chigrinov, V. G. *Liquid Crystal Devices: Physics and Applications*; Artech House: Boston, 1999.

(119) Wang, Q.; He, S. L.; Yu, F. H.; Huang, N. R. *Optical Engineering* **2001**, *40*, 2552.

(120) :. The correction factor of detection sensitivety is calculated by the averaged blips ratio of field on and field off at the Z= 3 micro meter.

(121) Negita, K. *Journal of Chemical Physics* **1996**, *105*, 7837.

(122) Ozaki, R.; Aoki, M.; Moritake, H.; Yoshino, K.; Toda, K. *Japanese Journal of Applied Physics Part 1-Regular Papers Brief Communications & Review Papers* **2006**, *45*, 4662.

(123) Loudet, J. C.; Hanusse, P.; Poulin, P. *Science* **2004**, *306*, 1525.

(124) Kawai, T.; Yoshihara, S.; Iwata, Y.; Fukaminato, T.; Irie, M. *ChemPhysChem* **2004**, *5*, 1606.

(125) Yin, Y.; Zhao, C.; Kuroki, S.; Ando, I. *Macromolecules* **2002**, *35*, 2335.

(126) van Bruggen, M. P. B.; Lekkerkerker, H. N. W.; Maret, G.; Dhont, J. K. G. *Phys. Rev. E* **1998**, *58*, 7668.

(127) Krueger, G. J. *Phys. Rep.* **1982**, *82*, 229.

(128) Stark, H.; Venttzki, D. *Phys. Rev. E* **2001**, *64*, 31711.

(129) Darinsjii, A. A.; Zarembo, A.; Balabaev, N. K.; Neelov, I. M.; Sundholm, F. *Phys. Chem. Chem. Phys.* **2003**, *5*, 2410.

(130) Hara, M.; Ichikawa, S.; Takezoe, H.; Fukuda, A. *Jpn. J. Appl. Phys.* **1984**, *23*, 1420.

(131) Spiegel, D. R.; Thompson, A. L.; Campell, W. C. *J. Chem. Phys.* **2001**, *114*, 3842.

(132) Urbach, W.; Hevet, H.; Rondelez, F. *J. Chem. Phys.* **1985**, *83*, 1877.

(133) Vasanthi, R.; Ravichandran, S.; Bagachi, B. *J. Chem. Phys.* **2001**, *114*, 7989.

(134) Loewen, H. *Phys. Rev. E* **1999**, *59*, 1989.

(135) Chu, K.-S.; Moroi, D. S. *J. Phys. (Paris), Colloq.* **1975**, *36*, C1.

(136) Hess, S.; Frenkel, D.; Allen, M. P. *Mol. Phys.* **1991**, *74*, 765.

(137) Etchegoin, P. *Phys. Rev. E* **1999**, *59*, 1860.

(138) Lettinga, M. P.; Barry, E.; Dogic, Z. *Europhys. Lett.* **2005**, *71*, 692.

(139) Brinkmeier, M.; Doerre, K.; Stephan, J.; Eigen, M. *Anal. Chem.* **1999**, *71*, 609.

(140) Schwille, P. *Cell Biochem. Biophys.* **2001**, *34*, 383.

(141) Elson, E. L.; Magde, D. *Biopolymers* **1974**, *13*, 1.

(142) Doi, M.; Edwards, S. F. *The Theory of Polymer Dynamics*; Clarendon Press: Oxford, 1986.

(143) Dvinskikh, S. V.; Furo, I. *J. Chem. Phys.* **2001**, *115*, 1946.

(144) Dvinskikh, S. V.; Furo, I.; Zimmermann, H.; Maliniak, A. *Phys. Rev. E* **2002**, *65*, 61701.

(145) Kirkwood, J. G.; Riseman, J. *J. Chem. Phys.* **1948**, *16*, 565.

(146) Tirado, M. M.; Garcia de la Torre, J. *J. Chem. Phys.* **1979**, *71*, 2581.

(147) Tirado, M. M.; Martinez, C. L.; Garcia de la Torre, J. *J. Chem. Phys.* **1984**, *81*, 2047.

(148) Ortega, A.; Garcia de la Torre, J. *J. Chem. Phys.* **2003**, *119*, 9914.

(149) Tang, S.; Evans, G. T. *Mol. Phys.* **1993**, *80*, 1443.

(150) Allison, S. A. *Macromolecules* **1999**, *32*, 5304.

Vita

Wei-Shun Chang was born in Taiwan on Novenber 4th 1973, the son of Yun-Ho Chang and Bi-Sha Chen. In 1992, he entered National Taiwan University as chemistry major, and received the degree of Bachelor of Science in 1996. Two years latter, he received the degree of Master of Science from the same University. After finishing the military service from 1998 to 2000, he joined Taiwan Semiconductor Manufacturing Company (TSMC) as a process engineer for about one and half years. In 2002, he stared his graduate work in the University of Texas at Austin with his supervisor Dr. Paul F. Barbara.

Permanent address: 119 Lancaster Dr. Clayton MO 63105

This dissertation was typed by Wei-Shun Chang